Key Points:
- Offshore Corinth Rift evolution is investigated at high spatial and temporal resolution
- Rift migration and localization of deformation are significant within the Corinth Rift
- Changes in rift geometry and linkage of major rift faults occur at rapid 100 kyr timescales

Supporting Information:
- Supporting Information S1

Correspondence to:
C. W. Nixon,
Casey.Nixon@uib.no

Rapid spatiotemporal variations in rift structure during development of the Corinth Rift, central Greece

Casey W. Nixon[1,2], Lisa C. McNeill[1], Jonathan M. Bull[1], Rebecca E. Bell[3], Robert L. Gawthorpe[2], Timothy J. Henstock[1], Dimitris Christodoulou[4], Mary Ford[5], Brian Taylor[6], Dimitris Sakellariou[7], George Ferentinos[4], George Papatheodorou[4], Mike R. Leeder[8], Richard E.Ll. Collier[9], Andrew M. Goodliffe[10], Maria Sachpazi[11], and Haralambos Kranis[12]

[1]National Oceanography Centre Southampton, University of Southampton, Southampton, UK, [2]Department of Earth Science, University of Bergen, Bergen, Norway, [3]Department of Earth Science & Engineering, Imperial College London, London, UK, [4]Department of Geology, University of Patras, Patras, Greece, [5]CRPG-CNRS, University of Nancy, Nancy, France, [6]School of Ocean and Earth Science and Technology, University of Hawai'i, Honolulu, Hawaii, USA, [7]Hellenic Centre for Marine Research, Anavissos, Greece, [8]School of Environmental Sciences, University of East Anglia, Norwich, UK, [9]School of Earth and Environment, University of Leeds, Leeds, UK, [10]Department of Geological Sciences, University of Alabama, Tuscaloosa, Alabama, USA, [11]National Observatory of Athens, Athens, Greece, [12]Dynamic, Tectonic and Applied Geology, National and Kapodistrian University of Athens, Athens, Greece

Abstract The Corinth Rift, central Greece, enables analysis of early rift development as it is young (<5 Ma) and highly active and its full history is recorded at high resolution by sedimentary systems. A complete compilation of marine geophysical data, complemented by onshore data, is used to develop a high-resolution chronostratigraphy and detailed fault history for the offshore Corinth Rift, integrating interpretations and reconciling previous discrepancies. Rift migration and localization of deformation have been significant within the rift since inception. Over the last circa 2 Myr the rift transitioned from a spatially complex rift to a uniform asymmetric rift, but this transition did not occur synchronously along strike. Isochore maps at circa 100 kyr intervals illustrate a change in fault polarity within the short interval circa 620–340 ka, characterized by progressive transfer of activity from major south dipping faults to north dipping faults and southward migration of discrete depocenters at ~30 m/kyr. Since circa 340 ka there has been localization and linkage of the dominant north dipping border fault system along the southern rift margin, demonstrated by lateral growth of discrete depocenters at ~40 m/kyr. A single central depocenter formed by circa 130 ka, indicating full fault linkage. These results indicate that rift localization is progressive (not instantaneous) and can be synchronous once a rift border fault system is established. This study illustrates that development processes within young rifts occur at 100 kyr timescales, including rapid changes in rift symmetry and growth and linkage of major rift faults.

1. Introduction

Over the past 20 years, numerous studies of synrift deformation have furthered our knowledge of fault and rift evolution, e.g., North Sea [*Fossen and Hesthammer*, 1998; *Cowie et al.*, 2005; *Bell et al.*, 2014], Gulf of Corinth Rift [e.g., *Taylor et al.*, 2011; *Ford et al.*, 2013], East African Rift [*Hayward and Ebinger*, 1996], Rio Grande Rift [*Leeder and Mack*, 2009], Gulf of Suez [*Gawthorpe et al.*, 2003], and Gulf of California [*Aragón-Arreola et al.*, 2005]. Studies of these evolving and mature rifts have recognized progressive strain localization as an important process in rift evolution on a variety of temporal and spatial scales. It is commonly thought that rifts develop an initially broad zone of complex deformation that becomes localized onto a smaller number of discrete and increasingly large faults [*Walsh et al.*, 2001; *Cowie et al.*, 2005], while sedimentation becomes focused into fewer, larger depocenters [*Gawthorpe and Leeder*, 2000; *Gawthorpe et al.*, 2003; *Cowie et al.*, 2007]. Furthermore, it has been shown that active faulting and strain migrate toward the rift axis with increasing extension, resulting in rift narrowing [*Gawthorpe et al.*, 2003; *Cowie et al.*, 2005]. Localization of deformation has also been predicted by both physical [e.g., *Ackermann et al.*, 2001; *Mansfield and Cartwright*, 2001] and numerical models [e.g., *Gupta et al.*, 1998; *Behn et al.*, 2002; *Huismans and Beaumont*, 2007].

Models of rift evolution are typically based on mature rifts and passive margins, where the first few million years of rift history are unresolved. Most studies have only achieved rift-scale temporal resolutions of the order of >1 Myr due to reliance on field observations (e.g., Gulf of Suez) [*Gawthorpe et al.*, 2003] or deep offshore basins (e.g., North Sea) [*Cowie et al.*, 2005]. Some studies have investigated the evolution of individual fault systems at
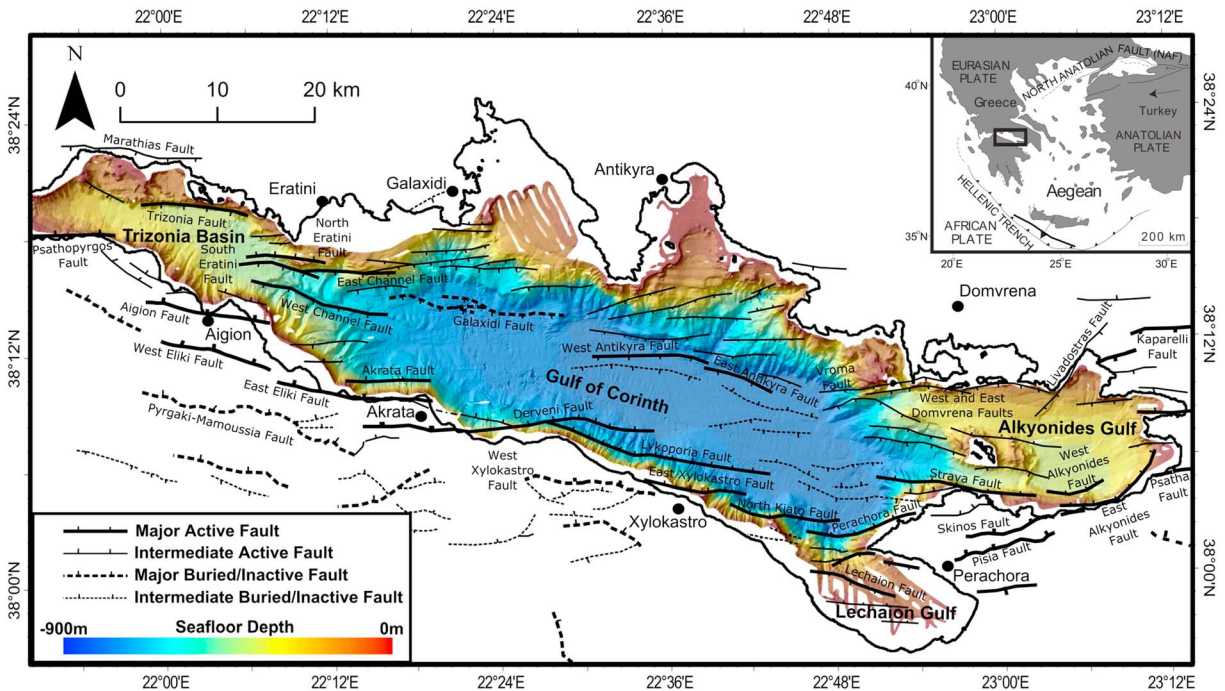
Figure 1. Structural map of the Corinth Rift, illustrating the new and refined offshore fault network interpreted in this study. Inset is a location map of the Corinth Rift within the tectonic framework of the Aegean. All major active faults offset 100 kyr horizon (see Figure 3). Onshore faults are after *Ford et al.* [2008] in the west, *Skourtsos and Kranis* [2009] for the central rift, and *Collier and Dart* [1991] and *Freyberg* [1973] in the east. Offshore faults in the Trizonia Basin are after *Beckers et al.* [2015]. Bathymetry data courtesy of the Hellenic Centre for Marine Research collected for R/V *Aegaeo* cruises [*Sakellariou et al.*, 2007].

finer spatial and temporal scale (tens of kiloyears); however, these studies have been restricted to recent activity only or are not at rift scale [e.g., *Morley et al.*, 2000; *Hemelsdaël and Ford*, 2014; *Nixon et al.*, 2014]. Therefore, details of variations in structural style, strain distribution, and strain rate at high resolution (temporal resolution of 10^4–10^6 years and spatial resolution of one to tens of kilometers) at whole rift scale are rarely resolved.

The Corinth Rift (Figure 1) initiated < 5 Ma [*Ori*, 1989] and is one of the most rapidly extending (10–16 mm/yr) [*Bernard et al.*, 2006; *Clarke et al.*, 1998; *Briole et al.*, 2000] active rift systems on Earth today. The rift itself is significantly smaller (~100 km × ~40 km) than other rifts (e.g., East African Rift; Basin and Range) and therefore can be investigated in its entirety at high resolution. The rift has a simple history of N-S extension [*McKenzie*, 1972; *Roberts and Jackson*, 1991] and has not been magmatically overprinted. Hence, this rift is an ideal natural laboratory for investigating the early development of marine/lacustrine rift basins and rifted margins.

The Corinth Rift has been studied extensively both onshore [e.g., *Gawthorpe et al.*, 1994; *Leeder et al.*, 2002, 2012; *Roberts et al.*, 2009; *Ford et al.*, 2013] and offshore [e.g., *Stefatos et al.*, 2002; *Sachpazi et al.*, 2003; *Leeder et al.*, 2005; *McNeill et al.*, 2005; *Lykousis et al.*, 2007; *Sakellariou et al.*, 2007; *Bell et al.*, 2008, 2009, 2011; *Taylor et al.*, 2011; *Charalampakis et al.*, 2014; *Beckers et al.*, 2015] to extract synrift sedimentation, fault and rift architecture, and to quantify extension. However, the existing marine seismic data sets have never been fully integrated, resulting in contrasting interpretations of the rift structure, the absence of a uniform stratigraphic framework for the offshore rift, and similar but inconsistent chronostratigraphic models [e.g., *Sachpazi et al.*, 2003; *Leeder et al.*, 2005; *Sakellariou et al.*, 2007; *Bell et al.*, 2008, 2009; *Taylor et al.*, 2011].

This paper integrates all available offshore Corinth Rift seismic reflection data (summarized in Figure 2), producing a dense network that is used to develop a uniform synrift stratigraphic and chronostratigraphic framework for the past circa 1–2 Myr. This framework allows us to unravel the structural development of the Corinth Rift at higher temporal resolutions than previously achieved here or at any other continental rift. We focus on quantifying variations in the distribution of the synrift sediments through time, illustrating the across- and along-strike development of the offshore rift structure and constraining the timeframes of switches in fault polarity and fault/depocenter linkage and localization. By quantifying the magnitude, rate, and timing of early rift deformation at unprecedented spatial resolutions and on timescales ≪1 Myr, we are
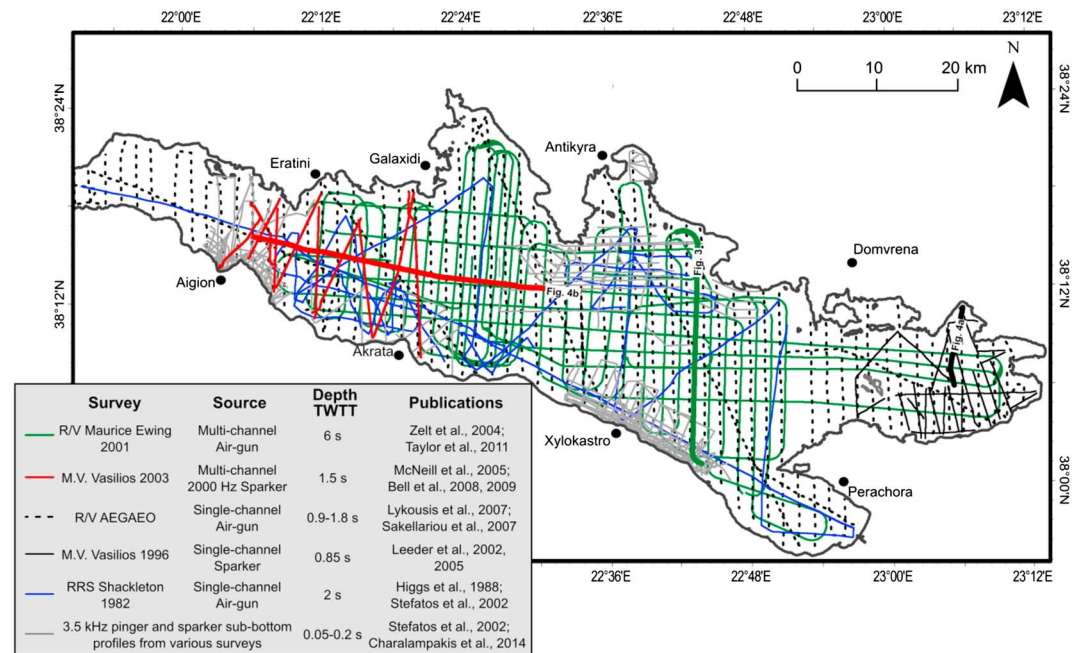
Figure 2. Map showing the locations of seismic reflection profiles and details of the seismic sources used to constrain the chronostratigraphy and fault geometry throughout the Corinth Rift. The locations of the interpreted seismic profiles in Figures 3 and 4 are also shown.

able to address the following key questions: How does rift geometry evolve and on what timescale? Is strain localization an abrupt or gradual process? And does it occur synchronously along a rift?

2. Geological Background and Stratigraphy of the Corinth Rift

The Corinth Rift forms a high strain band of N-S extension across central Greece that has been active since the late Pliocene [*Skourlis and Doutsos*, 2003; *Leeder et al.*, 2008; *Ford et al.*, 2013] (Figure 1), with the modern active rift axis (offshore Gulf of Corinth) initiating circa 2 Ma [e.g., *McNeill et al.*, 2005; *Bell et al.*, 2008, 2009; *Leeder et al.*, 2008]. Geodynamic models for the formation of the rift include extension associated with rollback of the subducting African Plate [*McKenzie*, 1978; *Doutsos et al.*, 1988; *Jolivet et al.*, 1994], gravitational collapse of overthickened crust [*Le Pourhiet et al.*, 2003], and the SW propagation of the dextral North Anatolian Fault [*Armijo et al.*, 1996, 1999]. Present-day geodetic rates of extension across the rift range from <5 mm/yr in the east to >10–15 mm/yr in the west [*Davies et al.*, 1997; *Clarke et al.*, 1998; *Briole et al.*, 2000; *Avallone et al.*, 2004]. However, long-term deformation patterns and whole-crust extension estimates indicate greater amounts of extension (~11–21 km) [*Bell et al.*, 2011] in the central rift and extension at lower rates in the western rift (0.6–4.8 mm/yr) [*Ford et al.*, 2013] in the past, indicating potentially significant temporal variations in strain distribution within the rift [*Bell et al.*, 2011; *Ford et al.*, 2013].

The onshore synrift sediments of the western and central rift have been separated into three lithostratigraphic groups: A Lower Group characterized by alluvial to lacustrine sediments deposited in the late Pliocene (estimated between circa 4 Ma and 2.5–1.8 Ma) during a time of distributed extension; a circa 2.5–1.8 Ma to 0.7–0.45 Ma Middle Group dominated by lacustrine fan deltas that built during a period of rift deepening and northward migration; and a circa 0.7–0.45 Ma to present Upper Group characterized by alternating marine and lacustrine sediments [e.g., *Ori*, 1989; *Gawthorpe et al.*, 1994; *Rohais et al.*, 2007; *Backert et al.*, 2010; *Leeder et al.*, 2012; *Ford et al.*, 2013]. Up to ~2.5 km of synrift sediments have accumulated in the offshore Gulf of Corinth. These comprise a deeper sequence (defined here as Seismic Unit 1, SU1) that varies considerably in thickness and largely lacks continuous coherent reflections and by a sequence (defined here as Seismic Unit 2, SU2) that is well stratified, consisting of laterally continuous packages of reflections [*Sachpazi et al.*, 2003; *Lykousis et al.*, 2007; *Bell et al.*, 2008, 2009; *Taylor et al.*, 2011] separated from SU1 by an unconformity. Analyses of sediment cores indicate alternating marine and lacustrine conditions in recent times, caused by basin isolation during glacial lowstands

Table 1. Comparison of Previous Chronostratigraphic Models Calculated for the Offshore Corinth Rift

Study	Region	Method	Identified Glacio-Eustatic Cycles	Unconformity Age Estimate
This Study	Entire Rift	Seismic Character and Clinoforms	6 × 100 kyr	~620 ka
Sachpazi et al. [2003]	Central Gulf of Corinth	Seismic Character	5 × 100 kyr	~500–600 ka
Bell et al. [2008]	Eratini Basin	Clinoforms	4 × 100 kyr	~400 ka
Bell et al. [2008, 2009]	Western Gulf of Corinth	Seismic Character	4 × 100 kyr	~300–400 ka
Taylor et al. [2011]	Central Gulf of Corinth	Seismic Character	7 × 100 kyr	~680 ka
Leeder et al. [2005]	Alkyonides Gulf	Clinoforms	5 × 100 kyr	~500 ka
Sakellariou et al. [2007]	Alkyonides Gulf	Seismic Character	4 × 100 kyr	~400–450 ka
Bell et al. [2009]	Alkyonides Gulf	Seismic Character & Clinoforms	6 × 100 kyr	~600 ka

by the Rion-Antirion sill in the west [e.g., *Perissoratis et al.*, 2000]. Analyzing seismic stratigraphy, previous studies have interpreted marine and lacustrine packages within SU2, correlating them with the Quaternary sea level, specifically 100 kyr glacio-eustatic cycles (different results summarized in Table 1) [*Sachpazi et al.*, 2003; *Moretti et al.*, 2004; *Leeder et al.*, 2005; *Lykousis et al.*, 2007; *Sakellariou et al.*, 2007; *Bell et al.*, 2008, 2009; *Taylor et al.*, 2011]. Thus, the existing tectonostratigraphic framework for the offshore Corinth Rift needs to be reconciled in order to accurately analyze sediment flux and fault activity history around the rift.

3. Methodology

3.1. Seismic Reflection Data

All available 2-D seismic reflection data from the offshore Corinth Rift were compiled and integrated, including high-resolution seismic, multichannel seismic, and scanned analogue data that cover a range of frequencies, totalling >5000 km of seismic profiles (summarized in Figure 2). Primarily, four seismic surveys were used for correlating faults and for the basin-wide chronostratigraphic interpretation:

1. R/V *Maurice Ewing 2001*—multichannel seismic (MCS) data penetrating the complete synrift sequence to basement throughout the Gulf, previously published by *Zelt et al.* [2004] and *Taylor et al.* [2011].
2. M.V. *Vasilios 2003*—High-resolution MCS data penetrating all or part of the synrift sequence in the western Gulf of Corinth, previously published by *McNeill et al.* [2005] and *Bell et al.* [2008, 2009].
3. R/V *AEGAO*—High-resolution single-channel data penetrating all or part of the synrift sequence throughout the Gulf previously published, in part, by *Lykousis et al.* [2007] and *Sakellariou et al.* [2007].
4. M.V. *Vasilios 1996*—High-resolution single-channel data in the Alkyonides Gulf previously published by *Collier et al.* [2000], *Leeder et al.* [2002, 2005], *Stefatos et al.* [2002], and *Bell et al.* [2009].

Local data sets including airgun profiles, single-channel sparker profiles, and subbottom profiles [e.g., *Stefatos et al.*, 2002; *Charalampakis et al.*, 2014] were used to confirm correlation and location of faults, in particular along the southern margin. Details of each seismic reflection survey can be found in the relevant publications listed in Figure 2.

3.2. Stratigraphic Interpretation

The dense network of seismic profiles allows us to accurately trace key seismic reflections within Seismic Unit 1 (SU1) and Seismic Unit 2 (SU2) throughout the offshore rift. We focus on areas east of Aigion where deep penetrating seismic data are present (Figures 1 and 2). The seismic stratigraphy is interpreted using the same techniques of previous studies (Table 1), specifically distinguishing marine and lacustrine packages within SU2:

1. Sedimentary structures and geometries: prograding clinoforms, truncation, and onlap on the upper slopes and shelf regions of the offshore rift. Following previous studies [e.g., *Leeder et al.*, 2005; *McNeill et al.*, 2005; *Bell et al.*, 2008, 2009], we interpret clinoforms as forming in lowstand, lacustrine conditions with onlapping marine sediments marking transgression.
2. Seismic character—In the main basin, changes in amplitude and frequency were used to divide the stratigraphy (methods of *Sachpazi et al.* [2003], *Lykousis et al.* [2007], *Bell et al.* [2008, 2009], and *Taylor et al.* [2011]), calibrated with Marion Dufresne long piston cores [*Moretti et al.*, 2004] sampling the last ~ 20–25 ka [see *Bell et al.*, 2008]. We use this method to identify lacustrine and marine packages within the seismic stratigraphy by picking the base horizon of higher amplitude packages, interpreted as the onset of marine sedimentation (e.g., Figure 3).
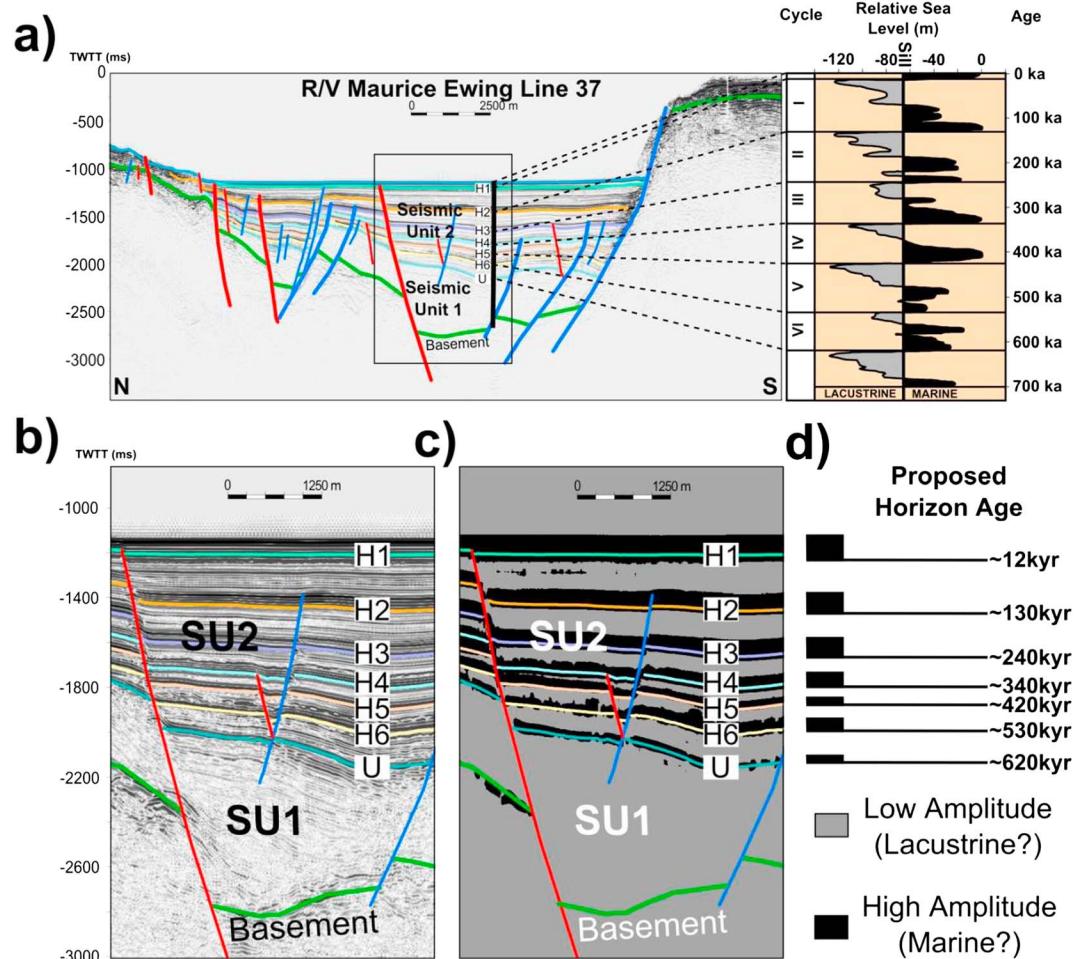
Figure 3. Corinth Rift chronostratigraphic framework, applicable to the entire rift, derived from analysis of data in Figure 2 which reconciles all previous interpretations. (a) Representative multichannel seismic reflection profile from the central Gulf of Corinth (R/V *Maurice Ewing 2001*) illustrating the seismic stratigraphy, modeled ages of alternating high and low-amplitude packages within the upper Seismic Unit 2 (SU2), and correlation with circa 100 kyr glacio-eustatic cycles. Packages are correlated to the sea level curve of *Bintanja and van de Wal* [2008] for the past circa 620 kyr. The current depth of the Rion Strait sill is indicated. Inset box indicates location of close-ups illustrated in Figures 3b and 3c. (b and c) Horizons (H1–H6, U) on a conventional seismic reflection profile and on a profile with an amplitude volume attribute applied to highlight the contrasting marine and lacustrine packages (high and low amplitude, respectively). (d) Proposed horizon age (<620 kyr) model for the Corinth Rift.

The alternating marine and lacustrine packages within SU2 can be correlated with circa 100 kyr glacio-eustatic cycles (sea level curve of *Bintanja and van de Wal* [2008]), providing age estimates for each stratigraphic horizon for the past circa 700 kyr. Proposed ocean drilling of the section will allow us to ultimately test the accuracy of this framework [*McNeill et al.*, 2014].

3.3. Sediment Distribution Analysis for Fault Activity

The SU2 stratigraphic horizons provide a high-resolution framework (1 km × 1 km; 100 kyr) to generate isochore maps and along-strike profiles of maximum sediment thickness. Sediment thicknesses are calculated using a linear velocity model (based on tomography data [*Zelt et al.*, 2004], prestacked depth migration [*Clement*, 2000], semblance plots [*Bell et al.*, 2008], and geophysical core logs [*Collier et al.*, 2000; *Moretti et al.*, 2004]) that increases at 1.5 km s^{-1} s^{-1} from the seafloor where the velocity is 1.55 km s^{-1} [*Moretti et al.*, 2004]. Sediments were decompacted using a porosity-depth relationship for calcareous sediments [*Goldhammer*, 1997]. Patterns in synrift sediment thickness were used to understand the links between fault and depocenter locations following an assessment of the contribution of fluvial sediment input to sediment thickness. Fault

polygon maps are used to illustrate the cumulative heave on faults for key time intervals. The length and width of the fault polygons are generated using hanging wall and footwall cutoff points and identifying realistic along-strike fault heave patterns. The fault polygons were superimposed onto the isochore maps allowing us to assess depocenter development and fault activity.

4. Uniform Stratigraphic Framework for the Offshore Corinth Rift

The two seismic units (SU1 and SU2) are separated by a basin-wide unconformity (horizon U), which marks an abrupt change in seismic character between the two units (e.g., Figure 3) [*Sachpazi et al.*, 2003; *Bell et al.*, 2009; *Taylor et al.*, 2011]. SU1 is characterized by lower amplitude reflections that lack coherency (Figure 3). In contrast, within SU2 we can clearly identify six high-amplitude marine packages (package bases H1–H6) and low-amplitude lacustrine packages, which we correlate with the last six circa 100 kyr glacio-eustatic cycles (Figure 3).

This chronostratigraphic interpretation is similar to that proposed by *Sachpazi et al.* [2003], but they do not recognize the most recent marine stage. Our interpretation matches *Taylor et al.* [2011] back to circa 480 ka; however, prior to circa 480 ka they compress sedimentation during the short lacustrine stage and surrounding marine stages of circa 620–480 ka into one reflection (our H6, Figure 3). *Taylor et al.* [2011] correlates the thick low-amplitude unit above the unconformity with the circa 680–620 ka lacustrine stage and the unconformity with the circa 710–680 ka marine stage. Instead, we allow for a local expansion of sedimentation during the short circa 560–530 ka lacustrine stage and correlate the unconformity with the onset of the circa 620–560 ka marine stage. Our model is preferred because (a) it maintains the correlation of high- and low-amplitude packages with marine and lacustrine conditions, respectively, and (b) it avoids significant changes in sedimentation rate. The unconformity and base of SU2 is therefore circa 620 ka (horizon U; Figure 3).

SU2 can be directly correlated into the Lechaion Gulf, consistent with the interpretations of *Taylor et al.* [2011] and *Charalampakis et al.* [2014]. Horizons for the last circa 240 kyr can also be correlated into the Alkyonides Gulf, matching well-defined clinoform interpretations of *Leeder et al.* [2005] and consistent with *Bell et al.* [2009] (Table 1 and Figure 4a). All SU2 horizons can be traced east to west along the whole Gulf of Corinth (Figure 4b) and are laterally continuous and conformable with the exception of the western Gulf, where H4 truncates underlying sediments forming a second unconformity. This is the unconformity interpreted by *Bell et al.* [2008, 2009], previously misinterpreted as being correlative with the older unconformity in the thicker central basin sequence. Therefore, there are two unconformities in the western Gulf of Corinth: the basin-wide SU1-SU2 unconformity at circa 620 ka and a younger unconformity at circa 340 ka local to the upper shelf and margins of the western Gulf of Corinth.

Our interpretation reconciles previous chronostratigraphic discrepancies (e.g., Table 1 and Figure 3d). Using the circa 620 ka age of the basin-wide unconformity (U) and the thickness of SU2 and SU1, we estimate an age of circa 1.5–2 Ma for the oldest sediments within the offshore rift using decompacted sedimentation rates of SU2, matching ages of *Bell et al.* [2009].

5. High-Resolution Along-Strike Rift Structure and Fault Network

In this section, we present and describe a new, highly detailed and more precise Corinth Rift fault map (Figure 1) with fault activity history and differences in the development of rift geometry along the rift (Figures 5 and 6 and Table 2). We divide the rift into five along-strike domains.

5.1. West Gulf of Corinth

The Trizonia Basin, west of Aigion (Figures 1 and 5), is predominantly controlled by the Psathopyrgos, Trizonia, and Aigion Faults [*Beckers et al.*, 2015]. East of Aigion, the southern margin is segmented into the active, en echelon, north dipping Aigion, Diakopto, West Eliki, and East Eliki Faults (Figure 5). Synrift sediments are mainly deposited in a narrow symmetrical graben primarily controlled by the south dipping West Channel Fault to the north and the north dipping Eliki Faults and currently inactive Pyrgaki-Mamoussia Faults to the south (Figures 5 and 6a). The laterally constant thickness between key horizons (i.e., basement, U, H4, and H2; Figure 6a) indicates approximately equal activity on the north and south bounding faults (Figure 5) during deposition of SU1 and SU2. In the footwall of the West Channel Fault,
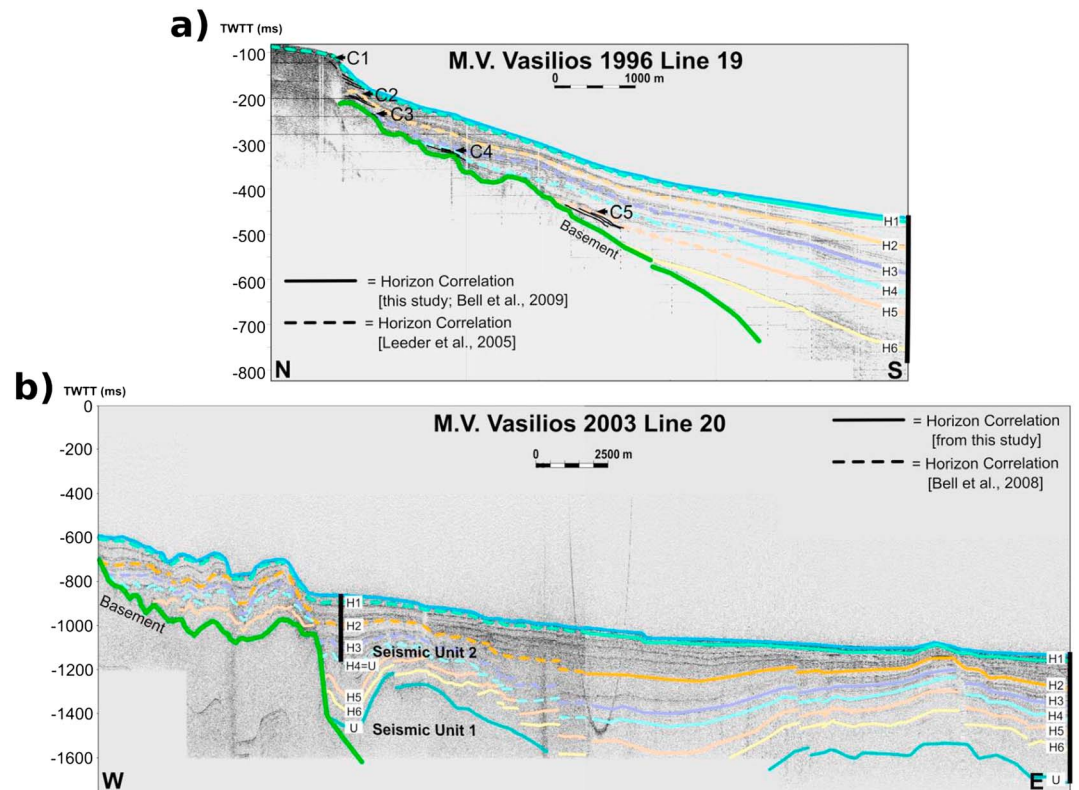
Figure 4. (a) Chronostratigraphic framework used in this study applied to a high-resolution seismic reflection profile from the Alkyonides Gulf. Note how the tops of clinoforms (C1–5; interpreted by *Leeder et al.* [2005]) correlate with the marine transgressive horizons (H1–H5) which represent the base of the high-amplitude marine packages. H6 is the base of the deepest marine package above unconformity U. This interpretation is consistent with *Bell et al.* [2009]. (b) West to east along-rift high-resolution seismic reflection profile illustrating how the chronostratigraphic framework from this study agrees with the interpretation of *Bell et al.* [2008]. The positions of profiles in Figures 4a and 4b are shown in Figure 2. Solid horizons represent interpretation from this study; dashed horizons are from previous studies. Uninterpreted profiles can be viewed in the supporting information.

the synrift sequence is significantly thinner, with only SU2 present, and horizon H4 becomes unconformable (Figure 6a). The South and North Eratini Faults, uplifting the northern horst block that forms the southern boundary of the Eratini subbasin, are interpreted as active since deposition of SU2 (circa 620 ka) (as per *McNeill et al.* [2005] and *Bell et al.* [2008]). The locus of rift-related subsidence stepped northward in this part of the rift at circa 620 ka, and, depending on the relative timing of the primary southern margin faults (Eliki and Derveni) and the Eratini Faults, the rift may have also widened. See also discussions by *Bell et al.* [2008], *Ford et al.* [2013], and *Taylor et al.* [2011].

5.2. Central West Gulf of Corinth

Along the northern margin a single large south dipping fault with a length of ~40 km has been named the East Channel or the Galixidi Fault [*Bell et al.*, 2008, 2009; *Taylor et al.*, 2011]; however, our denser seismic network shows that this fault is composed of multiple linked and unlinked segments. The segments that are fully linked at basement depth form what we now call the Galaxidi Fault (Figure 5). The remaining unlinked western fault segment ~8 km in length, situated between the West Channel Fault and the Galaxidi Fault, is now referred to as the East Channel Fault (Figure 5).

The synrift sediments deposited between the Derveni and Galaxidi Faults form an overall symmetrical graben but with a switch in fault dominance from south dipping to north dipping faults over time (Figure 6b) [*Sachpazi et al.*, 2003; *Bell et al.*, 2009; *Taylor et al.*, 2011]. Our new integrated data allow the extraction of details of this transition. The Galaxidi Fault was dominant during SU1 (Figure 6b and Table 2), but circa 620–340 ka a more symmetrical package of synrift sediments was deposited indicating a discrete transition period with equal north and south dipping fault activity (Figure 6b). Shortly after circa 340 kyr (horizon H4),
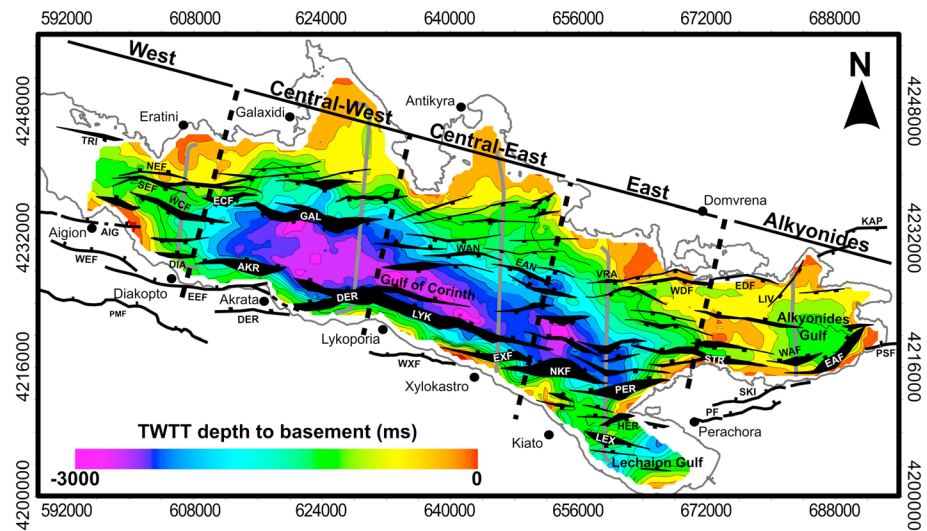
Figure 5. Fault map illustrating major faults offsetting seismic basement (depth illustrated by colored contours) with the width of the offshore fault polygons proportional to the heave on the faults. The down-throw direction of the faults is shown. The offshore Corinth Rift is divided into five domains from west to east to illustrate along-strike variation in rift architecture (see text for further description). The location of a representative seismic profile from each domain illustrated in Figure 6 is shown by the solid grey lines. Fault names: TRI = Trizonia Fault, NEF = North Eratini Fault, SEF = South Eratini Fault, WCF = West Channel Fault, ECF = East Channel Fault, AIG = Aigion, DIA = Diakopto, GAL = Galaxidi, PMF = Pyrgaki-Mamoussia Fault, EEF = East Eliki Fault, WEF = West Eliki Fault, AKR = Akrata, DER = Derveni, LYK = Lykoporia, EXF = East Xylokastro Fault, WXF = West Xylokastro Fault, NKF = North Kiato Fault, LEX = Lechaion, HER = Heraion, PER = Perachora, STR = Strava, WAF = West Alkyonides Fault, EAF = East Alkyonides Fault, LIV = Livadostras, EDF = East Domvrena Fault, WDF = West Domvrena Fault, VRA = Vroma, EAN = East Antikyra, WAN = West Antikyra.

the Galaxidi Fault became buried and inactive, coinciding with the formation of a south thickening half graben controlled by the north dipping Derveni Fault. The sediments of SU2 are deformed by numerous small south dipping faults between the Galaxidi and Derveni Faults (Figure 6b), often associated with an anticlinal structure that forms around a pivot point, potentially a damage zone related to the polarity reversal and transfer of strain.

5.3. Central East Gulf of Corinth

The Derveni Fault is hard linked to the Lykoporia Fault, forming a significant north dipping fault, ~40 km in length, bounding the southern margin of the central basin (Figures 5 and 6b). The now inactive West Xylokastro Fault (onshore) and active East Xylokastro Fault (offshore) both sit in the footwall of the Lykoporia Fault (Figure 5) [*Bell et al.*, 2009]. The northern margin is characterized by numerous smaller and less significant south dipping faults, including some previously unmapped faults on the shelf/slope that unusually trend NE-SW, with the main depocenter bound by the south dipping West and East Antikyra Faults (Figures 5 and 6c). A thin package of SU1 sediments (~300 ms two-way travel time (TWTT), <400 m thick) are deposited in a narrow symmetrical graben in this Domain (Figure 6c). Since circa 620 ka (SU2), the north dipping Lykoporia and East Xylokastro Faults have generated a half graben (Figure 6c), with the south dipping Antikyra Faults (WAN and EAN) on the northern margin less active. The minor south dipping faults in the footwall of the WAN and EAN appear to have activated during SU2 deposition, suggesting that the northern rift margin has stepped north during SU2.

5.4. East Gulf of Corinth

In the main basin during SU1 deposition, multiple basement horst structures are uplifted by south dipping faults creating small north thickening half graben [see *Bell et al.*, 2009]. The horsts became buried and inactive by circa 340 ka (Figure 6d). Along the southern margin of this basin, the north dipping North Kiato and Perachora Faults, ~12 km in length, form a dextral en echelon fault array with the East Xylokastro Fault which is probably linked at depth. In contrast to previous studies that interpret the Perachora Fault as a NE trending fault [e.g., *Stefatos et al.*, 2002; *Lykousis et al.*, 2007; *Bell et al.*, 2009; *Taylor et al.*, 2011; *Charalampakis et al.*, 2014],
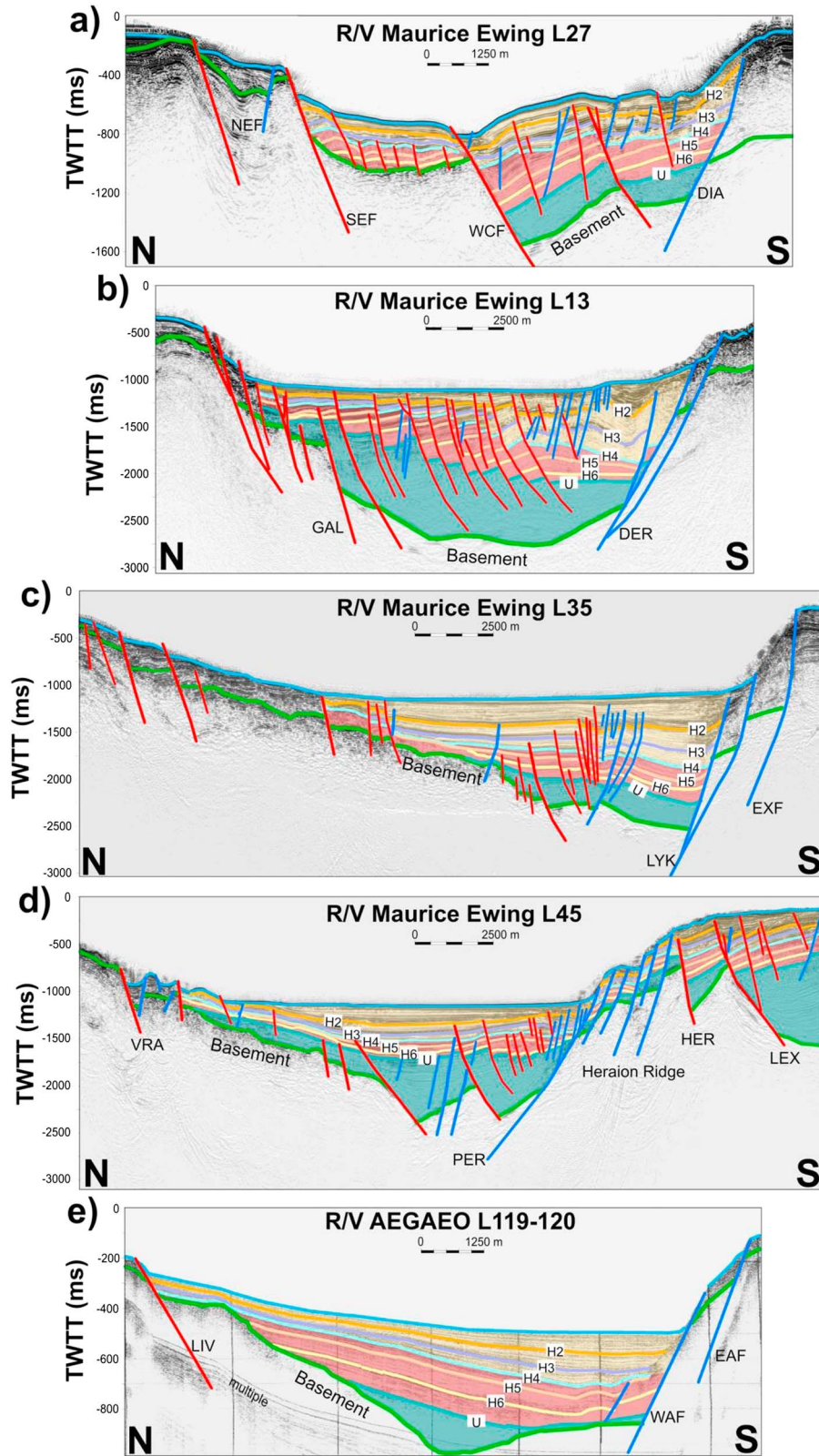
Figure 6. Interpreted seismic reflection profiles illustrating temporal-spatial changes in rift geometry and fault polarity along the Corinth Rift. (a–e) The West, Central West, Central East, East, and Alkyonides Domains shown in Figure 5, respectively. North and south dipping faults are shown in blue and red, respectively, see Figure 5 for fault nomenclature. Horizons H1–6 and U are labeled together with three synrift packages (yellow: seabed-H4; red: H4-U; blue: U-basement). See Table 2 for age correlation and summary of changes in fault polarity between rift domains. Uninterpreted profiles can be viewed in the supporting information.

Table 2. Summary of Rift Geometry Development for Domains Shown in Figures 5 and 6[a]

		West	Central West	Central East	East	Alkyonides
	Net Geometry	Symetrical Graben	Symetrical Graben	South Thickening Half Graben	South Thickening Half Graben	South Thickening Half Graben
~340-Present	Rift Geometry	Symetrical	South thickening	South thickening	South thickening	South thickening
	Controlling Faults	WCF, EEF	DER	LYK, XYL	NKF, PER	EAF
~620–340 kyr	Rift Geometry	Slightly north thickening	Symetrical	South thickening	Slightly south thickening	Symetrical
	Controlling Faults	WCF,EEF	GAL, DER	LYK, XYL	NKF, PER	EAF, LIV
~1.5 Ma to 620 kyr	Rift Geometry	Slightly north thickening	North thickening	Very little sediment	Numerous north thickening half grabens	Symetrical
	Controlling Faults	WCF, EEF, PMF	GAL	-	HER, LEX, Buried faults	EAF, LIV

[a]See Figure 5 caption for fault nomenclature.

we have identified its continuation closer to the Perachora Peninsula. This interpretation gives the Perachora fault an ENE trend, more consistent with adjacent faults. SU2 sediments thicken and tilt to the south, forming an asymmetrical graben controlled by the north dipping Perachora Fault (Figure 6d). The rift zone stepped north around circa 620 ka with upper SU1 and lower SU2 sediments draping the northern rift margin up to the south dipping Vroma Fault (Figures 5 and 6d).

The Heraion Ridge, bound by the Perachora Fault to the north and the Heraion and Lechaion Faults to the south (Figures 5 and 6d) [*Charalampakis et al.*, 2014], separates the Gulf of Corinth from the Lechaion Gulf. This ridge continues onshore at the Perachora Peninsula. In the Lechaion Gulf, SU1 and SU2 thicken in the hanging wall of the south dipping Heraion and Lechaion Faults, indicating their activity, and thin on top of the Heraion Ridge (Figure 6d) [see *Charalampakis et al.*, 2014].

5.5. Alkyonides Gulf

The Alkyonides Gulf is separated from the Gulf of Corinth by the fault-bounded horst of the Alkyonides Islands (Figure 5). The southern Alkyonides margin is controlled by the north dipping Strava, West Alkyonides, and East Alkyonides Faults [*Leeder et al.*, 2002, 2005; *Sakellariou et al.*, 2007]. The NE-SW trending Livadostras Fault controls the northern margin, and the West and East Domvrena Faults form a minor subbasin to the north of the Alkyonides Islands [see *Sakellariou et al.*, 2007; *Leeder et al.*, 2002; *Bell et al.*, 2009]. The Alkyonides Gulf forms an apparently simple south tilting half-graben structure dominated by north dipping faults (Figures 5 and 6e) [*Sakellariou et al.*, 2007; *Leeder et al.*, 2002; *Bell et al.*, 2009]. However, prior to circa 340 ka (below horizon H4; Figure 6e), uniform sediment thickness indicates equal activity on both south dipping and north dipping faults [see *Sakellariou et al.*, 2007]. Since circa 340 ka, the north to NW dipping West and East Alkyonides faults have dominated, generating the half graben (Figure 6e).

5.6. Summary of Along-Strike Rift Structure

Most along-strike rift domains show an evolution toward a simple south thickening half graben controlled by north dipping faults (Table 2 and Figure 6). The western Gulf of Corinth (Aigion to Diakopto) is the exception, with north and south dipping active faults forming a complex but symmetrical graben [e.g., *McNeill et al.*, 2005; *Bell et al.*, 2008]. The circa 620 ka unconformity (U) marks a major period of change in dominant fault polarity and rift symmetry with a transition period that lasted circa 300 kyr (circa 620–340 ka). At the end of this transition period, H4 (circa 340 ka) is unconformable in the western Gulf and major south dipping faults became inactive throughout the rift (Figure 6). After circa 620 ka, the northern rift margin stepped to the north throughout most of the Gulf of Corinth with minor south dipping faults activating north of the previous northern rift margin (Figure 7). This timing of increased strain distribution coincides with the switch in fault polarity at circa 620–340 ka.

6. Depocenter Development and Fault Linkage History—Refined and Improved Resolution

6.1. Primary Stages of Rift Depocenter Development

We have generated isochore maps for each synrift interval, building on the work of *Bell et al.* [2009] and *Taylor et al.* [2011], with significantly increased accuracy both temporally and spatially (Figures 7–9). Basement depth (Figure 5) indicates a single depocenter ~70 km in length (between Diakopto and Perachora) in the Central
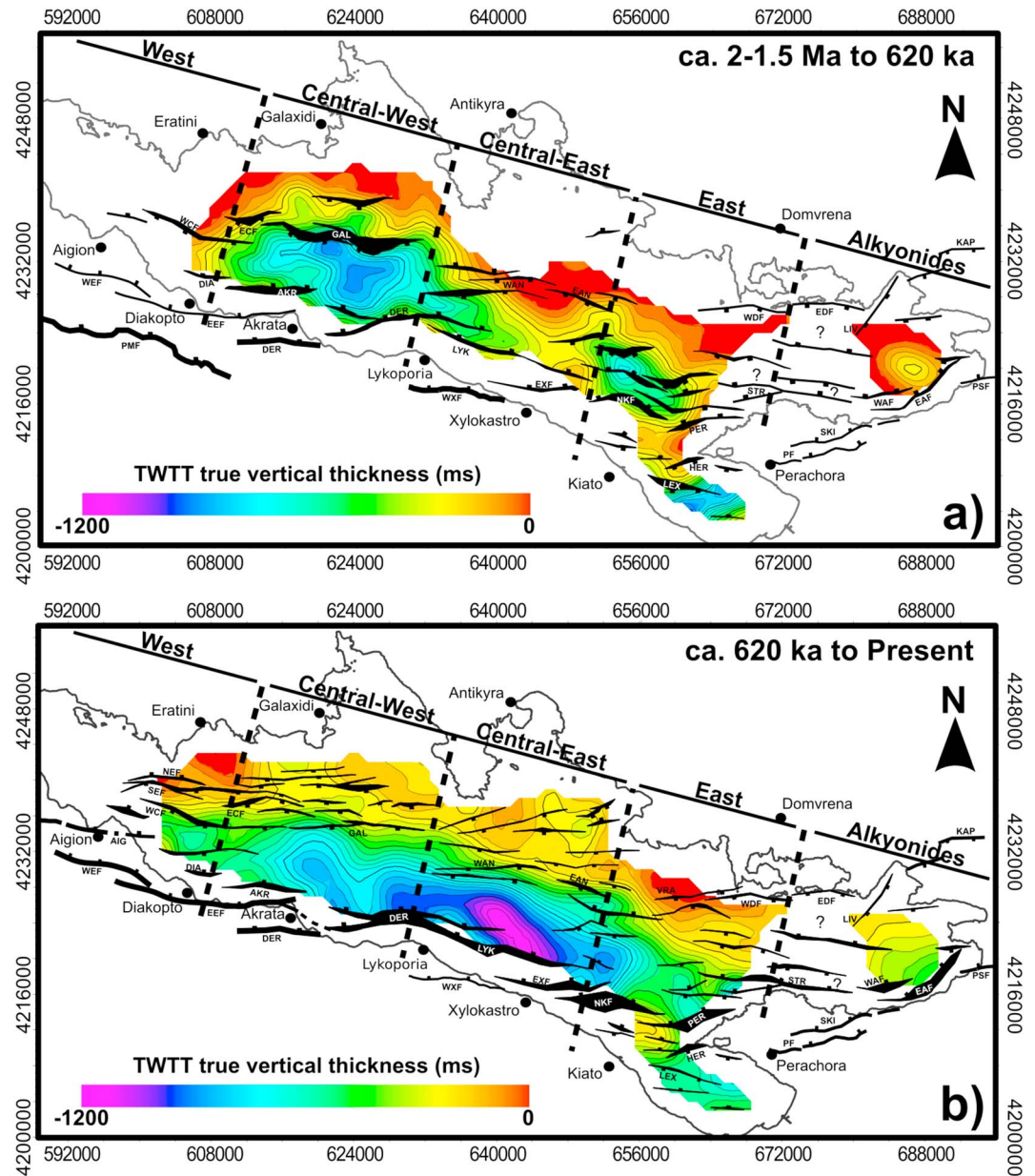
Figure 7. Isochore maps derived from the entire seismic reflection data set (Figure 2) for (a) Seismic Unit 1 (SU1; circa 1.5–2 Ma to 620 ka) and (b) Seismic Unit 2 (SU2; circa 620 ka to present day) illustrating major sediment depocenters and active faults. The fault polygons for each time period represent the cumulative heave on the faults within each time period. Fault nomenclature is as in Figure 5. Note the localized depocenters controlled by the Galaxidi Fault in the Central West Domain and both north and south dipping faults in the East Domain during before circa 620 ka. After circa 620 ka the major north dipping faults along the south shore of the Corinth Rift control the development of a laterally continuous depocenter (~50 km in length).

Domains (up to 3000 ms TWTT below sea level) with much shallower depths in the Alkyonides and West Domains (~1000 ms TWTT below sea level). The new isochore maps indicate (Figure 7) that before circa 620 ka (SU1; Figure 7a) synrift sediments were deposited in two separate depocenters: one in the hanging wall of the south dipping Galaxidi Fault (Central West Domain) and another bound by the north dipping North Kiato Fault and buried south dipping faults (East Domain). After circa 620 ka (SU2; Figure 7b) these depocenters became linked to form a single large depocenter, ~50 km in length, in the hanging walls of the north dipping Derveni, Lykoporia, and East Xylokastro Faults. Depocenter thickness is primarily influenced by sediment supply and creation of accommodation space. As discussed in the next section, sediment supply does not appear to play a significant role; thus, we can use thickness variations as a proxy for fault development.
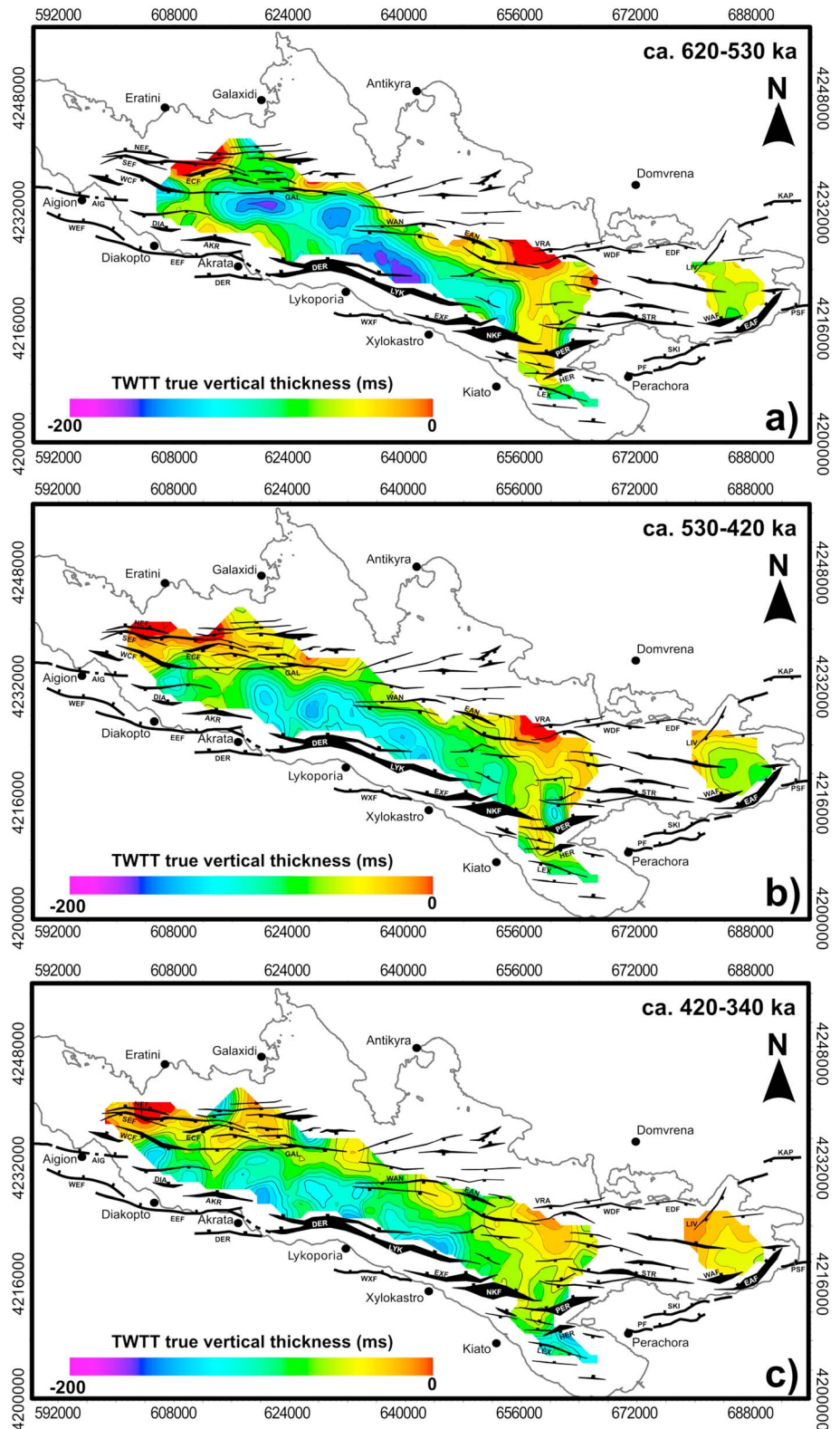
Figure 8. Isochore maps illustrating depocenter development over three time periods from circa 620–340 ka: (a) circa 620–530 ka; (b) circa 530–420 ka; and (c) circa 420–340 ka isochores. The fault polygons for each time period represent the cumulative heave on the faults since circa 620 ka. Initially (Figure 8a), discrete depocenters are controlled by both north and south dipping faults. This is followed by a gradual migration from north to south (Figures 8b and 8c) until all discrete depocenters are controlled by the southern margin north dipping faults (Figure 8c).
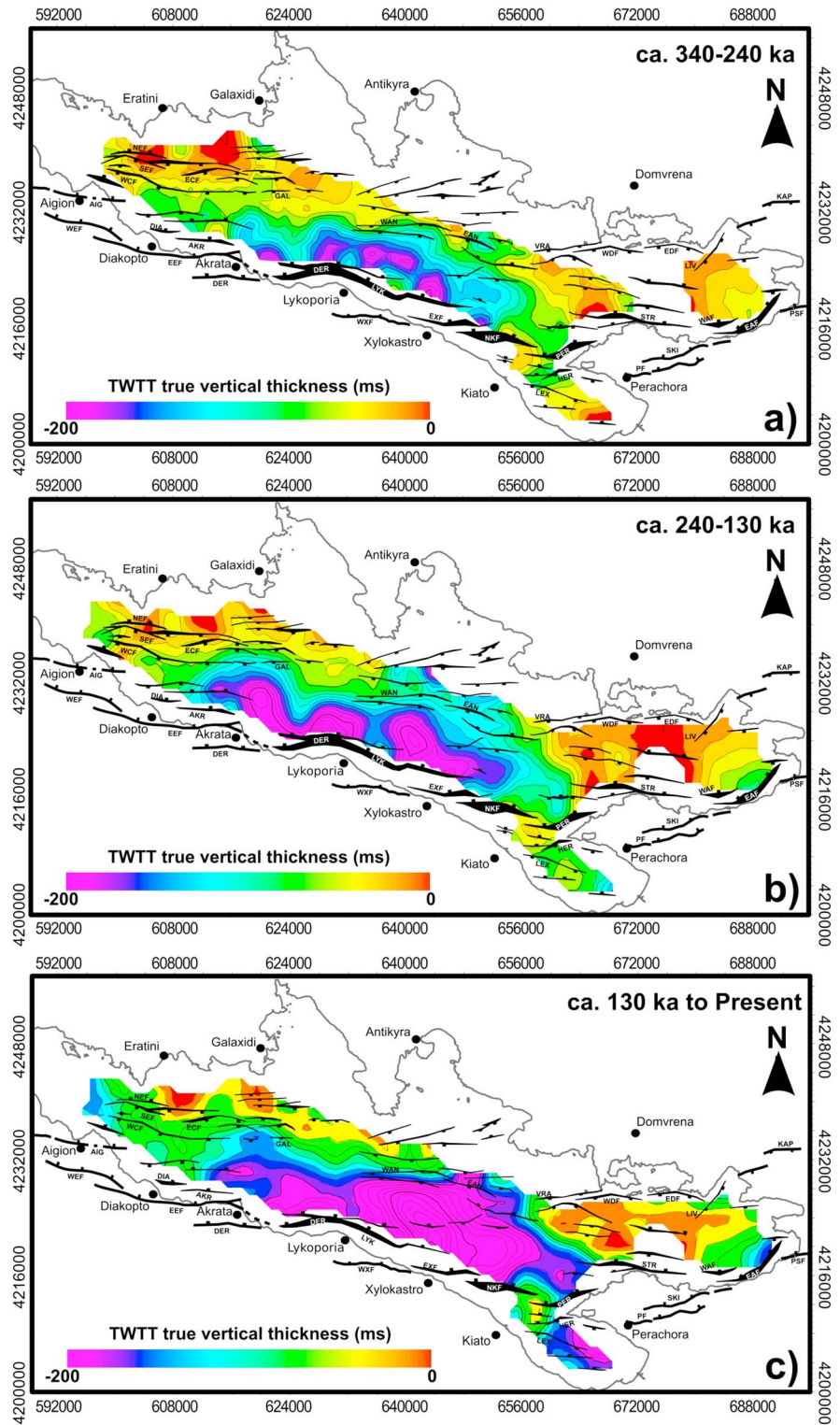
Figure 9. Isochore maps illustrating depocenter development over three time periods from circa 340 ka to the present day: (a) circa 340–240 ka; (b) circa 240–130 ka; and (c) circa 130 ka to present isochores. The fault polygons for time periods circa 340–130 ka and circa 130 ka to present represent the cumulative heave on the faults since circa 340 ka and circa 130 ka, respectively. Initially (Figure 9a), numerous small depocenters (~4–8 km in length) are controlled by discrete north dipping faults, along the southern margin of the Corinth Rift. These depocenters grow in size and become more linked with time (Figures 9b and 9c) eventually forming a large continuous depocenter ~40 km in length (Figure 9c), illustrating linkage of and localization on major north dipping faults.

Synrift sediment distribution indicates a major shift in rift structure from a complex rift zone controlled by both north and south dipping faults (Figure 7a), to a uniform asymmetric rift controlled by north dipping faults (Figure 7b). High-resolution 100 kyr interval isochore maps (Figures 8 and 9) highlight this establishment of an asymmetric rift over two phases: (1) a change in fault polarity over a discrete time interval (circa 100–300 kyr) between circa 620–340 ka and (2) linking of depocenters since circa 340 ka.

6.2. The Nature of the Switch in Fault Polarity

Between circa 620 and 340 ka (Figure 8), discrete depocenters were formed by both north dipping and south dipping faults (i.e., the Derveni and Lykoporia Faults and Galaxidi Fault, respectively). Initially (circa 620–530 ka), the depocenters were dominated by major south dipping faults; for example, the Galaxidi Fault controlled two discrete depocenters >200 ms TWTT (>250 m) thick in the north (Figure 8a). The depocenters progressively migrated southward during circa 530–420 ka with central maximum sediment accumulation (Figure 8b), and maximum sedimentation finally reached the southern rift margin and hanging walls of major north dipping faults (e.g., East Eliki and Derveni Faults) during circa 420–340 kyr (Figure 8c). This final stage (circa 420–340 ka) occurred along the entire length of the Gulf of Corinth southern margin (i.e., East Eliki, Derveni, Lykoporia, and East Xylokastro Faults; Figure 8c). The East Alkyonides Fault also began to dominate sediment deposition in the Alkyonides Gulf during this time interval (Figure 8c). Thus, north dipping faults have dominated subsidence and deposition throughout the active rift zone, creating a uniform asymmetric offshore rift since circa 340 ka. The depocenters migrated southward at a rate of ~30 m/kyr suggesting a progressive strain transfer.

6.3. Depocenter Growth and Linkage Since Circa 340 ka

Since circa 340 ka, discrete depocenters in the hanging walls of the north dipping East Eliki, Derveni, Lykoporia and East Xylokastro Faults have started to grow and link (Figure 9a). Major south dipping faults have become buried and inactive and in some cases propagated upward as smaller fault segments (e.g., Galixidi Fault; Figure 9a), no longer influencing depocenter development.

Between circa 340 and 240 ka (Figure 9a), a number of small discrete depocenters, ~4 km in length with ~200 ms TWTT (~250 m) sediment thickness formed in the hanging walls of the East Xylokastro, Lykoporia and Derveni Faults and between the now linked Derveni and East Eliki Faults. These discrete depocenters grew in size, increasing in length at a rate of ~40 m/kyr to form three partially linked depocenters, ~8–12 km in length with >200 ms TWTT (>250 m) sediment thickness, by circa 240–130 ka (Figure 9b). The Perachora Fault also generated a smaller depocenter in the eastern Gulf of Corinth during this time period.

The depocenters grew substantially from circa 130 ka to present day (Figure 9c), linking to form a major depocenter ~40 km in length with up to 400 ms TWTT (~400 m) of post-130 ka accumulated sediments. The depocenter offshore Akrata was smaller with relatively high subsidence offshore Lykoporia. Overall, the most significant region of sediment accumulation shifted eastward, to offshore Xylokastro (Figures 9c and 10). The Alkyonides Gulf depocenter (in the hanging wall of the West and East Alkyonides Faults) also increased in relative thickness. Therefore, since circa 340 ka, depocenters along the southern margin of the offshore Corinth Rift have increased in size, thickness, and degree of linkage, reflecting the localization of deformation and linkage of the major north dipping fault system that bounds the southern margin.

6.4. Quantifying Offshore Sediment Accumulation and Depocenter Development

The major spatial shifts in distribution of synrift sediments is further illustrated by along-strike profiles of maximum sediment thickness (Figure 10). Depocenter development is influenced by a combination of hanging wall subsidence and sediment supply. Present-day major river systems and associated deltas are evenly distributed along the Peleponesse coastline (Figure 10). The positions of these river systems can be fault controlled [e.g., the Krathis River; *Hemelsdaël and Ford*, 2014], but their positions for the most part do not align with peaks in maximum sediment accumulation rate, which vary temporally and are often coincident with the center of individual fault segments (Figures 10d and 10e). Thus, sediment input does not appear to be the most important control on patterns of synrift sediment thickness. Instead, sediment distribution appears to be predominantly fault controlled and, with sufficient sedimentation rates, should be an accurate measure of the growth and activity of major basin-bounding faults (e.g., Figure 10) and basin subsidence.
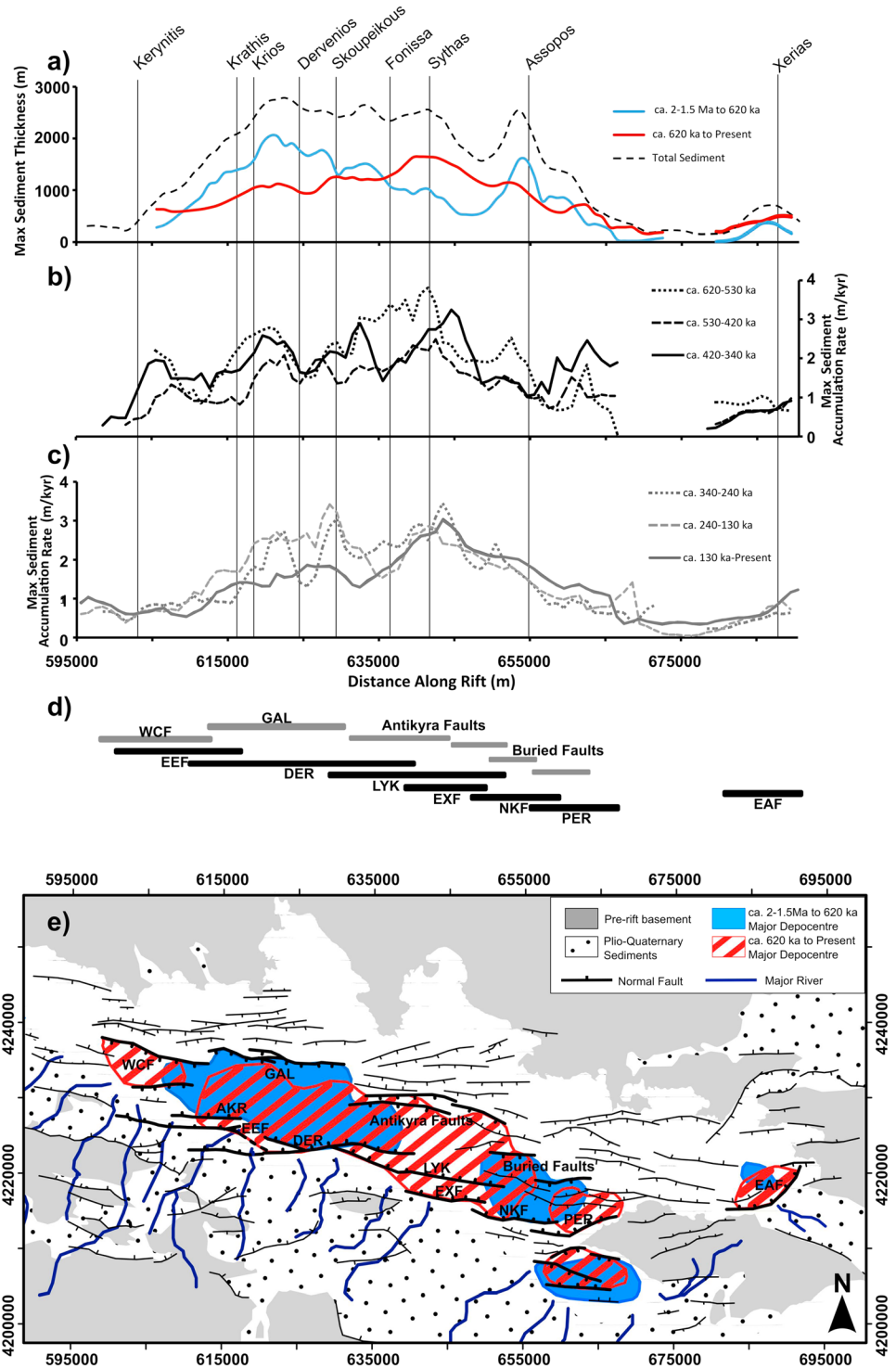
Figure 10. Spatial and temporal changes in the loci of sediment deposition within the offshore Corinth Rift. (a) Changes in the maximum decompacted sediment thickness for the major time periods. Note the change from two major depocenters before circa 620 ka to a single broad depocenter after circa 620 ka (blue and red, respectively). The present shoreline locations of major rivers are shown and labeled. (b and c) The change in maximum decompacted sedimentation rate along the rift for six circa 100 kyr glacio-eustatic cycles. The along-rift sedimentation becomes more uniform with time. (d) Schematic map showing positions of major controlling faults in the Gulf of Corinth and Alkyonides Gulf. North and south dipping faults are shown in black and grey, respectively. (e) Changes in the loci of sedimentation before and since circa 620 ka (blue and red stripe areas offshore, respectively). Positions of major faults are shown in bold as well as locus of onshore Plio-Quaternary sedimentation and outcrop of prerift basement.

Table 3. Comparison of the Assigned Age Estimates for Boundaries Within the Onshore and Offshore Stratigraphic Models[a]

	Onshore Stratigraphic Model		Offshore Stratigraphic Model	
Stratigraphic Group	Age Estimates	Study	Stratigraphic Unit	Age Estimates
----------------	circa 4–3.6 Ma	*Rohais et al.* [2007]	----------------	
Lower Group			???	
----------------	circa 2.5–1.8 Ma	*Leeder et al.* [2012]; *Ford et al.* [2013]	----------------	circa 2–1.5 Ma
Middle Group			Seismic Unit 1	
----------------	circa 0.7–0.45 Ma	*Ford et al.* [2013]; *Rohais et al.* [2007]	----------------	circa 0.6 Ma
Upper Group			Seismic Unit 2	
----------------	Present day		----------------	Present day

[a]See text for discussion.

From circa 2–1.5 Ma to 620 ka (SU1), variations in the maximum unit thickness show peaks in sediment accumulation at ~625,000 m and ~655,000 m (UTM coordinates; Figure 10b), coinciding with the two depocenters (Figure 7a). However, maximum sediment thickness for SU2 (circa 620 ka – present) is at ~640,000 m (UTM coordinates; Figure 10b), directly between the two peaks of SU1, illustrating the shift in sediment accumulation toward the center of the rift due to depocenter linkage (Figure 7b). The combined effect of these two phases produces a maximum total sediment thickness distribution with a flattened bell-curved shape (Figure 7a) over the last 1.5–2 Myr.

Comparison of maximum sediment accumulation rates for different time intervals since circa 620 ka (Figures 10c and 10d) show that overall rates have been relatively constant, averaging 1–3 m/kyr and sufficient to record deformation despite an underfilled present-day basin. However, within each circa 100 kyr interval there are more localized peaks in maximum sediment accumulation rate, coincident with the depocenters in the major basin-bounding fault hanging walls (i.e., Figure 10e).

The maximum sediment accumulation rate profiles combined with isochore maps (Figures 8 and 9) indicate that the overall shift in sediment distribution and depocenter development occurs gradually over the past 620 kyr. During circa 620–340 ka, the peaks in maximum rate change from being quite irregular in size and distribution (i.e., circa 620–530 ka; Figure 10c) to forming five consistent peaks that are evenly distributed and similar in size (i.e., circa 420–340 ka; Figure 10c), reflecting the change in fault polarity/rift symmetry (Figure 8). Since circa 340 ka there are a smaller number of peaks in the profiles of maximum sediment rate that eventually form a broad bell-curved profile with a central peak at 645,000 m (UTM coordinates; Figure 10d), representing the growth and linkage of the faults and depocenters (Figure 9).

7. Summary of Corinth Rift Evolution From Inception Circa 4 Ma to Present

The onshore stratigraphic model of Lower, Middle, and Upper Groups [*Rohais et al.*, 2007; *Ford et al.*, 2013; *Leeder et al.*, 2012] is widely used, but limited datable material means that there are no absolute ages for the boundaries between the groups and discrepancies exist between studies. Therefore, we use a range of ages for each group that encompass these age estimates (Table 3) and apply the broad chronology to the rest of the onshore rift.

Our proposed ages for seismic stratigraphic units SU1 (circa 2–1.5 Ma to 0.6 Ma) and SU2 (circa 0.6 Ma to present) chronologically correspond with the age estimates for the Middle Group (circa 2.5–1.8 Ma to 0.7–0.45 Ma) and Upper Group (circa 0.7–0.45 Ma to present), respectively (Table 3) [*Rohais et al.*, 2007; *Leeder et al.*, 2012; *Ford et al.*, 2013]. Combined with new insights of offshore fault activity and previously published onshore fault activity, this correlation allows us to refine the general evolution of the Corinth Rift over the last circa 4 Myr (Figure 11).

7.1. Late Pliocene to Early Pleistocene (Circa 4 Ma to 2.5–1.8 Ma)

The earliest synrift sediments (circa 4–3.6 Ma [*Rohais et al.*, 2007]), within the Lower Group, occurred onshore and were deposited in a rift with distributed faulting and significant inherited relief [*Collier and Jones*, 2003; *Ford et al.*, 2007, 2013; *Rohais et al.*, 2007]. The majority of the Lower Group sediments (Figure 11a) were defined by a series of north dipping faults, including the Dhemesticha and Kalavryta Faults, and possibly a buried south dipping fault in the western rift [*Ford et al.*, 2013; *Wood et al.*, 2015];
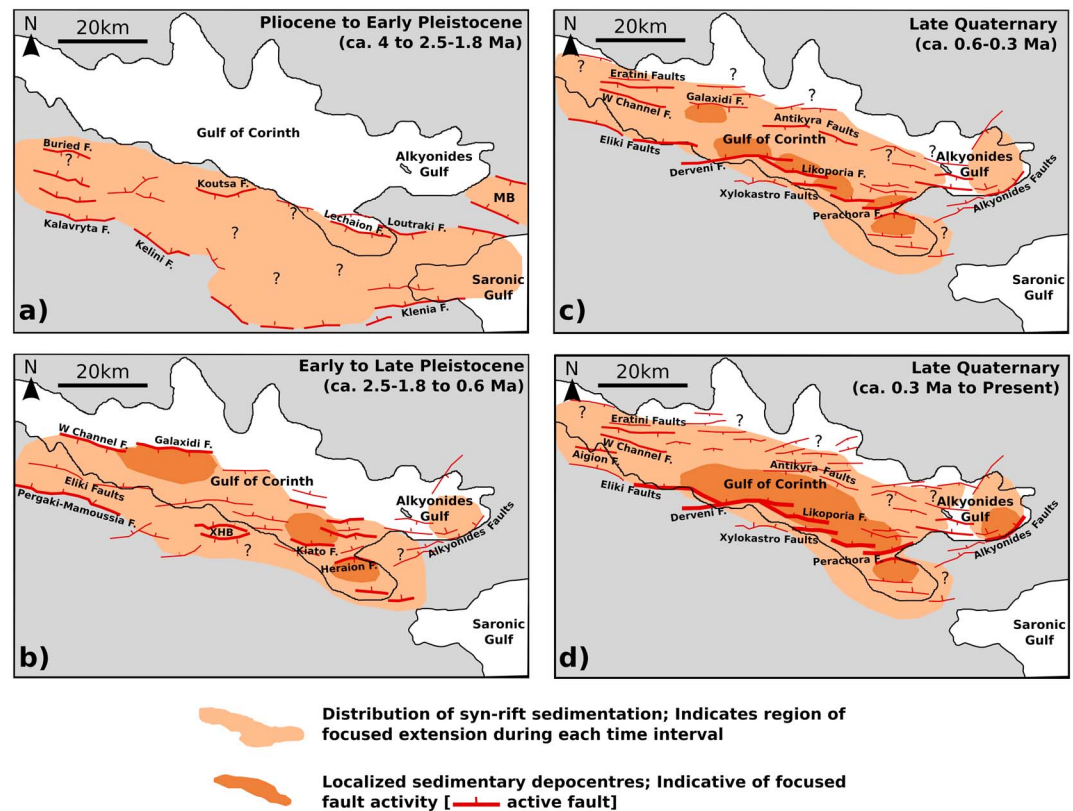
Figure 11. Plan view maps indicating evolution of Corinth Rift from inception circa 4 Ma to present day. Inferred fault activity based on new insights from this study, previous offshore studies [*McNeill et al.*, 2005; *Bell et al.*, 2008, 2009], and correlations with recent onshore studies [*Leeder et al.*, 2008, 2012; *Ford et al.*, 2013; *s.*, 2014]. The distribution of well-constrained synrift sediments is shown for each time period indicating the region of focused extension. See text for discussion of rift evolution.

the Kellini Fault and the Koutsa Fault/Xylokastro Horst block in the central rift [*Leeder et al.*, 2008, 2012]; and the Klenia Fault and Loutraki/Lechaion Faults in the eastern rift, which marked the northern margin of the Corinth-Nemea basin [*Collier and Dart*, 1991; *Charalampakis et al.*, 2014]. Our age correlation suggests that the Lower Group sediments are minimal/absent offshore suggesting little or no deformation and associated subsidence there before circa 2 Ma [*Bell et al.*, 2009]; however, this cannot be confirmed without direct sampling. In the Alkyonides Gulf the onshore synrift sediments formed in the NW-SE trending Megara basin at this time [*Leeder et al.*, 2008], and equivalent sediments are likely in the base of the eastern Alkyonides basin either fault bound or infilling preexisiting basement topography [*Sakellariou et al.*, 2007].

7.2. Early Pleistocene to Late Pleistocene (Circa 2.5–1.8 Ma to Circa 0.6 Ma)

Deformation migrated northward [*Leeder et al.*, 2008; *Ford et al.*, 2013] and became more focused onto individual north and south dipping faults during deposition of the Middle Group [*Ford et al.*, 2007; *Rohais et al.*, 2007; *Bell et al.*, 2009]. A major depocenter in the western rift was bound by the onshore Pyrgaki-Mamoussia Fault along the southern margin and controlled by the offshore Galaxidi Fault (Figure 11b) [*Ford et al.*, 2013]. In the central rift, our data indicate minimal sedimentation offshore Xylokastro at this time, likely due to the onshore Xylokastro Horst Block confining Gilbert fan delta deposits to the south (Figure 11b) [*Leeder et al.*, 2012]. Deformation was apparently accommodated by a number of south dipping faults, including the Heraion Fault, in the eastern rift (Figure 11b) [*Charalampakis et al.*, 2014]. In the Megara basin, deformation ceased and transferred northwest to the Alkyonides Gulf between circa 0.8 and 2.2 Ma with initiation of north to NW dipping faults on the southern margin of the Alkyonides Gulf [*Leeder et al.*, 2008].

7.3. Late Quaternary (Circa 0.6 Ma to Present)

The rift migrated farther north with the majority of Upper Group sediments deposited in the modern offshore rift (Figures 11c and 11d). Major south dipping faults (i.e., Galaxidi Fault) decreased in activity between circa
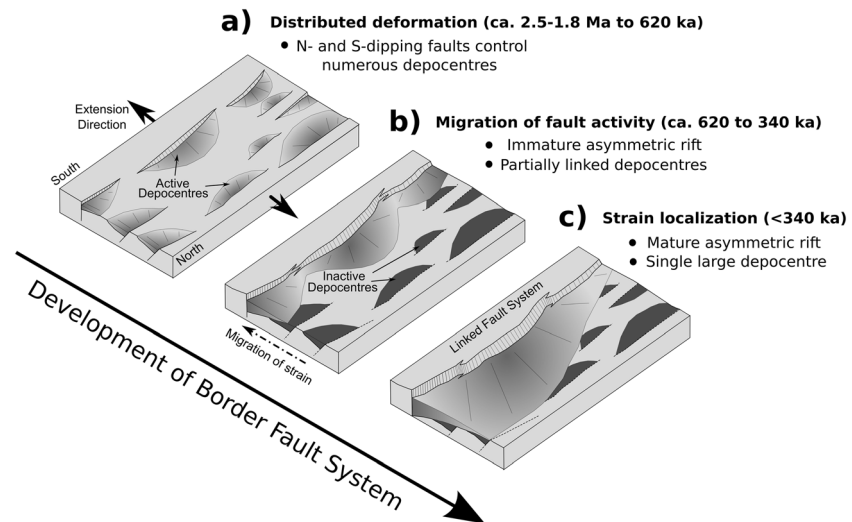
Figure 12. Three-dimensional diagrams illustrating the development of a rift border fault system and associated depocenters.

620 and 340 ka, and depocenters became focused along the southern margin (Figure 11c). The western rift is an exception because of activation of the north and south dipping Eratini Faults [*McNeill et al.*, 2005; *Bell et al.*, 2008, 2009], whereas deformation in the central rift became focused on the north dipping Derveni, Lykoporia, and Xylokastro Faults. The eastern rift was characterized by numerous horst blocks as the north dipping Perachora Fault also became more active. Since circa 340 kyr, the major north dipping faults, such as the Eliki, Derveni, Lykoporia, Xylokastro, and Perachora Faults, have increased in activity to control a single major depocenter along the southern margin of the Gulf of Corinth. In contrast, deformation of the northern margin is now taken up by numerous distributed south dipping faults (Figure 11d). In the Alkyonides Gulf, deformation has become focused on the north dipping East Alkyonides Fault, and the Heraion Fault continues to control deposition in the Lechaion Gulf.

8. Discussion

This is one of the first studies of its kind to look at key rift evolutionary processes such as rift geometry evolution, depocenter development, and fault linkage at such unprecedented resolutions (~100 kyr and ~1 km) across an entire rift and can now be compared with different models of rift development and with more mature rift systems.

8.1. Rapid Changes in Fault Polarity and Rift Symmetry

The development of asymmetry in a rift zone is relatively common, for example, in much of the East African rift zone [*Ebinger and Scholz*, 2012]. Many studies have documented spatial variability in fault polarity and rift symmetry within rifts, including the Gulf of Suez [*Patton et al.*, 1994; *Bosworth et al.*, 2005], East Africa [*Rosendahl*, 1987; *Hayward and Ebinger*, 1996], the now inactive North Sea [*Cowie et al.*, 2000], and fully evolved passive margin settings [*Mohammed et al.*, 2016]. Models indicate that rift development should be spatially and temporally variable due to variations in fault timing and activity, with rifts developing from numerous isolated basins to a single laterally continuous half graben [e.g., *Cowie et al.*, 2000]. Such models show a consistent dominant fault polarity throughout rift development. However, our observations from the offshore Corinth Rift indicate a spatially complex rift zone with both north and south dipping faults dominating at different times, before forming a uniform asymmetric rift controlled by north dipping faults (Figures 7–9).

For the first time we can constrain the rate of polarity and symmetry change within a rift and determine the discrete time interval for this process in parts of the rift. We show that this is a rapid but progressive (rather than instantaneous) process, taking place over a time interval as small as 300 kyr. The transition to a more simple asymmetric rift is characterized by a decrease in activity and death of major south dipping faults as strain is transferred onto major north dipping faults. For example, in the Central West Domain of the rift, strain transfers from the Galaxidi Fault to the Derveni Fault (Figures 8b, 12a, and 12b). The decrease in activity of

major south dipping faults results in the local unconformity observed within their footwall blocks in the western rift at circa 340 kyr (e.g., Figure 6a). An accommodation zone of numerous conjugate minor faults forms around a pivot point in the rift axis at this time of polarity/symmetry change (Figure 6b). Similar conjugate zones of distributed deformation have been documented and are thought to show interaction between domains of differing fault polarity [e.g., *Nelson et al.*, 1992; *Fossen and Hesthammer*, 1998; *Kornsawan and Morley*, 2002; *Schlische and Withjack*, 2009; *Nixon et al.*, 2011]. The polarity change across the rift results in north to south migration of depocenters (Figures 8 and 12) toward the southern margin and the hanging walls of the major rift border faults (Figures 11 and 12b).

Although asymmetry within the rift develops over a particular period, the resolution of our data set allows us to determine that asymmetry does not develop synchronously along strike (Figure 6 and Table 2). Major north dipping faults have dominated in the Central East and East Domains since circa 620 ka forming south thickening half graben (Figures 6c and 6d and Table 2), whereas deformation in the Central West Domain and the Alkyonides was not dominated by north dipping faults until circa 340 ka (Figures 6b and 6e and Table 2). The West Domain is still structurally complex with a symmetrical graben controlled by both north and south dipping faults (Figure 6a and Table 2). Possible links between West Domain structure and preexisting basement structure and composition are discussed below.

8.2. Timescales of Growth and Linkage of the Rift Border Fault System

Border fault systems are common in most rift systems [e.g., *Ebinger*, 1989; *Schlische*, 1993]; however, the timescales of their development are not well understood. In the Corinth Rift, we can now constrain these timescales. The southern margin of the modern Corinth Rift is characterized by numerous right stepping en echelon north dipping faults that make up the border fault system (Figure 5). Small and partially linked depocenters form in the hanging wall of many of these faults by circa 340 ka (Figures 8 and 9). Over time these depocenters show diachronous growth in size and thickness (Figure 9b) eventually merging to form a single large depocenter (Figure 9c). Similar synrift sediment distributions have been seen in a number of rift basins recording the growth and linkage of rift fault systems [e.g., *Schlische*, 1993; *Gupta et al.*, 1998; *Morley*, 1999; *Contreras et al.*, 2000; *Wilson et al.*, 2009] but at lower resolutions and with less precise chronostratigraphic frameworks than presented here.

The profiles of maximum sediment accumulation rate (Figures 10c and 10d) reflect hanging wall subsidence patterns of the major north dipping faults along the southern rift margin. Initial along-strike variations in subsidence evolve to a centered but flattened bell-curve distribution (Figure 10d), consistent with accumulation of displacement on coalescing fault segments that form a kinematically coherent fault system seen in other extensional systems (Figures 12b and 12c) [e.g., *Peacock and Sanderson*, 1991; *Dawers and Anders*, 1995; *Gupta and Scholz*, 2000; *Walsh et al.*, 2003a; *Taylor et al.*, 2004]. Hence, the individual en echelon north dipping faults are likely to be linked at depth along the entire Gulf of Corinth (but disconnected from the Alkonides Gulf). The growth and linkage of discrete depocenters, increasing in length by ~40 m/kyr, suggests that individual faults initially grew by rapid tip propagation before breaching of relay zones during segment linkage (Figures 12b and 12c). These observations are consistent with observations by *Hemelsdaël and Ford* [2014] who show evidence for fault propagation and linkage of the East Eliki and Derveni Faults at the Akrata relay zone circa 700–200 ka. This model of fault growth by propagation and segment linkage is at variance with instantaneous fault growth models where faults maintain a constant length and do not propagate as displacement builds [e.g., *Childs et al.*, 1995; *Walsh et al.*, 2002; *Paton*, 2006].

Although the fault and depocenter linkage is a progressive process, it occurred rapidly and synchronously along strike over a relatively short 300–500 kyr time interval (Figure 12). Similar time scales of segment linkage are seen on the Rangitaiki Fault in the Whakatane Graben, which has evolved from isolated fault segments to a single coherent fault system over a period of circa 400 kyr [*Taylor et al.*, 2004; *Bull et al.*, 2006; *Nixon et al.*, 2014]. The rapid linkage and establishment of a coherent border fault system is attributed to localization of deformation, a common observation of other rift fault systems [e.g., *Morley*, 1999; *Gawthorpe et al.*, 2003; *Walsh et al.*, 2003b; *Cowie et al.*, 2005; *Soliva and Schultz*, 2008] but rarely quantified.

8.3. Controls on Migration, Localization, and Along-Strike Variations in Rift Development

Rift migration, localization of deformation, and evolution toward a simpler rift structure are significant processes in establishing the Corinth Rift structure. The following sequential evolutionary stages are

identified (see Figure 11): (1) major northward migration of the rift (Figures 11a and 11b), (2) minor northward migration of the rift and a major change in rift symmetry toward asymmetry and development of the border fault system (Figures 11b and 11c), and (3) rapid linkage and establishment of a coherent border fault system and associated depocenters, and localization of strain onto the border fault system (Figures 11c and 11d).

The northward migration of the rift is sustained by sequential fault activity on both margins. *Ford et al.* [2013] illustrated this for the southern margin of the western Corinth Rift with migration between north dipping faults (i.e., Kalavryta Fault to the Eliki Fault; Figures 11a–11c). Similar observations are seen at a number of margins including Iberia and Namibia [*Ranero and Pérez-Gussinyé*, 2010; *Mohammed et al.*, 2016]. For example, at the Iberian margin brittle deformation is accommodated by sequentially active faults that young and dip oceanward [e.g., *Wilson et al.*, 2001; *Ranero and Pérez-Gussinyé*, 2010]. *Manatschal and Bernoulli* [1999] propose that margin migration is driven by lithospheric cooling and strengthening during rifting. More recent thermomechanical models suggest that rift migration is controlled by lower crustal flow and that the extent of migration is a function of crustal rheology, strain softening, and initial thermal structure [*Brune et al.*, 2014]. In Corinth, this early migration process may also be linked to the dynamics of the underlying subducting plate [e.g., *Tiberi et al.*, 2000; *Le Pourhiet et al.*, 2003; *Leeder et al.*, 2003]; however, these other margin examples demonstrate that the process of migration can be part of the intrinsic rifting process.

Localization of deformation is consistent with both modeling results [e.g., *Behn et al.*, 2002; *Huismans and Beaumont*, 2007] and other rift examples, including the Gulf of Suez and northern North Sea [e.g., *Gawthorpe et al.*, 2003; *Cowie et al.*, 2005]. However, these studies tend to observe migration of fault activity and localization toward the rift axis resulting in significant rift narrowing. In Corinth, a narrowing of the rift is not observed through time as indicated by the well-constrained distribution of synrift sediments (illustrated in Figure 11) [*Ford et al.*, 2013]. Instead, fault activity (although relatively minor) is maintained away from the zone of localization (the southern margin border fault system) as both southern and northern margins migrate northward. Lithospheric-scale numerical models suggest that rift narrowing is caused by increasing geothermal gradients associated with lithosphere thinning [*Behn et al.*, 2002] and/or frictional-plastic strain softening localizing on inherited weaknesses [*Huismans and Beaumont*, 2007]. The absence of rift narrowing suggests that these processes are not (yet?) dominant in the Corinth Rift, which maintains a narrow rift zone (20–40 km wide) throughout its history indicative of relatively low temperatures and a consequently strong lithosphere rheology [e.g., *Buck*, 1991; *Brun*, 1999].

Despite spatial and temporal variations in rift geometry and position over the last circa 2 Ma, the Corinth Rift has clearly evolved toward a uniform asymmetric rift with deformation localized onto a few major north dipping faults. The West Domain is the exception with strain still distributed across numerous north and south dipping faults and a contrasting evolution of strain rate relative to the rest of the rift with present-day extensional strain high in the west but relatively low in the past [e.g., *Bell et al.*, 2011]. Variations in rift development can be caused by differences in underlying basement structure and composition through reactivation of preexisting structures [e.g., *Paton et al.*, 2006] and/or pervasive strength anisotropy deflecting the local stress field and affecting fault geometry [e.g., *Morley*, 2010; *Corti et al.*, 2013]. In Corinth, crustal thickness and basement composition/structure vary from east to west across the Hellenide fold-thrust belt that trends NNW-SSE across the Corinth Rift [e.g., *Skourtsos and Kranis*, 2009]. In the Central East and East Domains (Figure 5), an ESE structural fabric exists within the Parnassos nappe potentially preconditioning the basement for the localization and development of large E-W trending normal faults [*Taylor et al.*, 2011]. However, in the Central West and West Domains (Figure 5), the Pindos nappe exhibits a strong NNW structural fabric that is highly oblique to the normal fault trends, hence potentially inhibiting fault growth and favoring segmentation. This could contribute to the structural complexity and apparently immature rift development in the West Domain of the Gulf of Corinth.

In general, rift models fail to show many of the processes we have observed in the Corinth Rift, particularly the switch in fault polarity. This could be a result of the temporal resolution of numerical models which are typically on million year timescales [e.g., *Huismans and Beaumont*, 2007; *Brune et al.*, 2014]. Furthermore, some of these processes could be reflecting driving mechanisms associated with the Corinth Rift, such as the influences of the subducting slab or nearby major lithospheric boundaries (e.g., the North Anatolian Fault) that

would change strain boundary conditions. Such influences on rifting are common and yet are typically not incorporated into numerical models, which use simple extensional boundary conditions, and thus should be considered for future modeling scenarios.

9. Conclusions

Using the largest seismic reflection data set available, we have generated a unified stratigraphic and structural framework for the entire offshore Corinth Rift. We document variations in rift depocenter development and fault activity at unprecedented 100 kyr time scales, producing a high-precision history of rift evolution over the past circa 2 Myr.

The most significant structural change is the rapid transition from a structurally complex rift to a predominantly asymmetric rift over a 300 kyr period, starting at circa 620 ka. Since circa 620 ka, two phases of offshore rift development have dominated: (1) a change in rift symmetry and then (2) progressive localization of deformation. The change in rift symmetry involved rapid (~200–300 kyr period) yet progressive transfer of deformation from south dipping to north dipping faults causing depocenter migration and the generation of a basin-wide synrift unconformity. Depocenters developing in the hanging walls of the north dipping faults grew laterally at rates of ~40 m/kyr as the uniform asymmetric rift became established at circa 340 ka. Growth and linkage of individual north dipping faults controlled depocenter development, and a coherent, linked border fault system was established rapidly (over a 300–500 kyr period) resulting in a single depocenter by circa 130 ka with maximum sediment accumulation now in the center of the rift.

This study illustrates that shifts in strain distribution within rifts can occur rapidly, on 100 kyr timescales. Strain localization can be synchronous throughout a rift once a uniform asymmetry has been established, allowing rapid growth and linkage of faults to form the rift border fault system. This process is progressive and can occur very early in a rift's history, in this case <4–5 Myr into rift history. We show that the rate of fault and depocenter linkage can be measured at very high temporal (circa 100 kyr) and spatial (circa 1 km) resolutions, where sediment supply is sufficient. Rift migration, an evolution toward asymmetry rather than symmetry, and a rapid change in dominant fault polarity within a rift are not typically generated in simple rift models yet may be a significant part of the rift evolution process.

References

Ackermann, R. V., R. W. Schlische, and M. O. Withjack (2001), The geometric and statistical evolution of normal fault systems: An experimental study of the effects of mechanical layer thickness on scaling laws, *J. Struct. Geol.*, *23*(11), 1803–1819, doi:10.1016/S0191-8141(01)00028-1.

Aragón-Arreola, M., M. Morandi, A. Martín-Barajas, L. Delgado-Argote, and A. González-Fernández (2005), Structure of the rift basins in the central Gulf of California: Kinematic implications for oblique rifting, *Tectonophysics*, *409*(1-4), 19–38, doi:10.1016/j.tecto.2005.08.002.

Armijo, R., B. Meyer, G. C. P. King, A. Rigo, and D. Papanastassiou (1996), Quaternary evolution of the Corinth Rift and its implications for the Late Cenozoic evolution of the Aegean, *Geophys. J. Int.*, *126*(1), 11–53, doi:10.1111/j.1365-246X.1996.tb05264.x.

Armijo, R., B. Meyer, A. Hubert, and A. Barka (1999), Westward propagation of the North Anatolian fault into the northern Aegean: Timing and kinematics, *Geology*, *27*(3), 267–270, doi:10.1130/0091-7613(1999)027.

Avallone, A., P. Briole, A. M. Agatza-Balodimou, H. Billiris, O. Charade, C. Mitsakaki, A. Nercessian, K. Papazissi, D. Paradissis, and G. Veis (2004), Analysis of eleven years of deformation measured by GPS in the Corinth Rift Laboratory area, *C. R. Geosci.*, *336*(4-5), 301–311, doi:10.1016/j.crte.2003.12.007.

Backert, N., M. Ford, and F. Malartre (2010), Architecture and sedimentology of the Kerinitis Gilbert-type fan delta, Corinth Rift, Greece, *Sedimentology*, *57*(2), 543–586, doi:10.1111/j.1365-3091.2009.01105.x.

Beckers, A., A. Hubert-Ferrari, C. Beck, S. Bodeux, E. Tripsanas, D. Sakellariou, and M. De Batist (2015), Active faulting at the western tip of the Gulf of Corinth, Greece, from high-resolution seismic data, *Mar. Geol.*, *360*, 55–69, doi:10.1016/j.margeo.2014.12.003.

Behn, M. D., J. Lin, and M. T. Zuber (2002), A continuum mechanics model for normal faulting using a strain-rate softening rheology: Implications for thermal and rheological controls on continental and oceanic rifting, *Earth Planet. Sci. Lett.*, *202*(3-4), 725–740, doi:10.1016/S0012-821X(02)00792-6.

Bell, R. E., L. C. McNeill, J. M. Bull, and T. J. Henstock (2008), Evolution of the offshore western Gulf of Corinth, *Geol. Soc. Am. Bull.*, *120*(1-2), 156–178, doi:10.1130/B26212.1.

Bell, R. E., L. C. McNeill, J. M. Bull, T. J. Henstock, R. E. L. Collier, and M. R. Leeder (2009), Fault architecture, basin structure and evolution of the Gulf of Corinth Rift, central Greece, *Basin Res.*, *21*(6), 824–855, doi:10.1111/j.1365-2117.2009.00401.x.

Bell, R. E., L. C. McNeill, T. J. Henstock, and J. M. Bull (2011), Comparing extension on multiple time and depth scales in the Corinth Rift, Central Greece, *Geophys. J. Int.*, *186*(2), 463–470, doi:10.1111/j.1365-246X.2011.05077.x.

Bell, R. E., C. A.-L. Jackson, P. S. Whipp, and B. Clements (2014), Strain migration during multiphase extension: Observations from the northern North Sea, *Tectonics*, *33*, 1936–1963, doi:10.1002/2014TC003551.

Bernard, P., et al. (2006), Seismicity, deformation and seismic hazard in the western rift of Corinth: New insights from the Corinth Rift Laboratory (CRL), *Tectonophysics*, *426*(1-2), 7–30, doi:10.1016/j.tecto.2006.02.012.

Bintanja, R., and R. S. W. van de Wal (2008), North American ice-sheet dynamics and the onset of 100,000-year glacial cycles, *Nature*, *454*, 869–872.

Bosworth, W., P. Huchon, and K. McClay (2005), The Red Sea and Gulf of Aden Basins, *J. Afr. Earth Sci.*, *43*(1-3), 334–378, doi:10.1016/j.jafrearsci.2005.07.020.

Briole, P., A. Rigo, H. Lyon-Caen, J. C. Ruegg, K. Papazissi, C. Mitsakaki, A. Balodimou, G. Veis, D. Hatzfeld, and A. Deschamps (2000), Active deformation of the Corinth Rift, Greece: Results from repeated Global Positioning System surveys between 1990 and 1995, *J. Geophys. Res.*, *105*(B11), 25,605–25,625, doi:10.1029/2000JB900148.

Brun, J. (1999), Narrow rifts versus wide rifts: Inferences for the mechanics of rifting from laboratory experiments, *Philos. Trans. R. Soc., A*, *357*(1753), 695–712, doi:10.1098/rsta.1999.0349.

Brune, S., C. Heine, M. Pérez-Gussinyé, and S. V. Sobolev (2014), Rift migration explains continental margin asymmetry and crustal hyper-extension, *Nat. Commun.*, *5*, 4014, doi:10.1038/ncomms5014.

Buck, W. R. (1991), Models of continental lithosphere extension, *J. Geophys. Res.*, *96*(B12), 161–178, doi:10.1029/91JB01485.

Bull, J. M., P. M. Barnes, G. Lamarche, D. J. Sanderson, P. A. Cowie, S. K. Taylor, and J. K. Dix (2006), High-resolution record of displacement accumulation on an active normal fault: Implications for models of slip accumulation during repeated earthquakes, *J. Struct. Geol.*, *28*(7), 1146–1166, doi:10.1016/j.jsg.2006.03.006.

Charalampakis, M., V. Lykousis, D. Sakellariou, G. Papatheodorou, and G. Ferentinos (2014), The tectono-sedimentary evolution of the Lechaion Gulf, the south eastern branch of the Corinth graben, Greece, *Mar. Geol.*, *351*, 58–75, doi:10.1016/j.margeo.2014.03.014.

Childs, C., J. Watterson, and J. J. Walsh (1995), Fault overlap zones within developing normal fault systems, *J. Geol. Soc. London*, *152*, 535–549.

Clarke, P. J., et al. (1998), Crustal strain in central Greece from repeated GPS measurements in the interval 1989–1997, *Geophys. J. Int.*, *135*(1), 195–214, doi:10.1046/j.1365-246X.1998.00633.x.

Clement, C. (2000), Imagerie sismique crustale de la subduction Hellenique et du Golfe de Corinth PhD thesis, Univ. Paris VII, Paris.

Collier, R., and G. Jones (2003), Rift sequences of the southern margin of the Gulf of Corinth (Greece) as exploration/production analogues AAPG Int. Conf.

Collier, R. E. L., and C. J. Dart (1991), Neogene to Quaternary rifting, sedimentation and uplift in the Corinth Basin, Greece, *J. Geol. Soc. London*, *148*(6), 1049–1065, doi:10.1144/gsjgs.148.6.1049.

Collier, R. E. L., M. R. Leeder, M. Trout, G. Ferentinos, E. Lyberis, and G. Papatheodorou (2000), High sediment yields and cool, wet winters: Test of last glacial paleoclimates in the northern Mediterranean, *Geology*, *28*(11), 999–1002, doi:10.1130/0091-7613(2000)28<999:HSYACW>2.0.CO;2.

Contreras, J., M. H. Anders, and C. H. Scholz (2000), Growth of a normal fault system: Observations from the Lake Malawi basin of the east African rift, *J. Struct. Geol.*, *22*(2), 159–168, doi:10.1016/S0191-8141(99)00157-1.

Corti, G., M. Philippon, F. Sani, D. Keir, and T. Kidane (2013), Re-orientation of the extension direction and pure extensional faulting at oblique rift margins: Comparison between the Main Ethiopian Rift and laboratory experiments, *Terra Nova*, *25*(5), 396–404, doi:10.1111/ter.12049.

Cowie, P. A., S. Gupta, and N. H. Dawers (2000), Implications of fault array evolution for synrift depocentre development: Insights from a numerical fault growth model, *Basin Res.*, *12*(3-4), 241–261.

Cowie, P. A., J. Underhill, M. Behn, J. Lin, and C. Gill (2005), Spatio-temporal evolution of strain accumulation derived from multi-scale observations of Late Jurassic rifting in the northern North Sea: A critical test of models for lithospheric extension, *Earth Planet. Sci. Lett.*, *234*(3-4), 401–419, doi:10.1016/j.epsl.2005.01.039.

Cowie, P. A., G. P. Roberts, and E. Mortimer (2007), Strain localization within fault arrays over timescales of 10^0–10^7 years, in *Tectonic Faults: Agents of Change on a Dynamic Earth*, pp. 47–78, MIT Press, Cambridge, Mass.

Davies, R., P. England, B. Parsons, H. Billiris, D. Paradissis, and G. Veis (1997), Geodetic strain of Greece in the interval 1892–1992, *J. Geophys. Res.*, *102*(B11), 24,571–24,588, doi:10.1029/97JB01644.

Dawers, N. H., and M. H. Anders (1995), Displacement—Length scaling and fault linkage, *J. Struct. Geol.*, *17*, 607–614.

Doutsos, T., N. Kontopoulos, and G. Poulimenos (1988), The Corinth-Patras rift as the initial stage of continental fragmentation behind an active island arc (Greece), *Basin Res.*, *1*(3), 177–190.

Ebinger, C., and C. Scholz (2012), Continental rift basins: An East African perspective, in *Tectonics of Sedimentary Basins, Recent Adv.*, vol. 185–208, edited by C. Busby and A. Azor, 647 pp., Wiley-Blackwell, Chichester, U. K.

Ebinger, C. J. (1989), Geometric and kinematic development of border faults and accommodation zones, Kivu-Rusizi rift, Africa, *Tectonics*, *8*(1), 117–133, doi:10.1029/TC008i001p00117.

Ford, M., C. Le Carlier de Veslud, and O. Bourgeois (2007), Kinematic and geometric analysis of fault-related folds in a rift setting: The Dannemarie basin, Upper Rhine Graben, France, *J. Struct. Geol.*, *29*(11), 1811–1830, doi:10.1016/j.jsg.2007.08.001.

Ford, M., E. A. Williams, F. Malartre, and S.-M. Popescu (2008), Stratigraphic architecture, sedimentology and structure of the Vouraikos Gilbert-type fan delta, Gulf of Corinth, Greece, *Int. Assoc. Sediment. Spec. Publ.*, *38*, 49–90.

Ford, M., S. Rohais, E. A. Williams, S. Bourlange, D. Jousselin, N. Backert, and F. Malartre (2013), Tectono-sedimentary evolution of the western Corinth Rift (Central Greece), *Basin Res.*, *25*(1), 3–25, doi:10.1111/j.1365-2117.2012.00550.x.

Fossen, H., and J. Hesthammer (1998), Structural geology of the Gullfaks Field, northern North Sea, *Geol. Soc. London Spec. Publ.*, *127*(1), 231–261, doi:10.1144/GSL.SP.1998.127.01.16.

Freyberg, B. von (1973), Geologie des Isthmus von Korinth, *Erlanger Geol. Abh.*, *95*, 183.

Gawthorpe, R. L., and M. R. Leeder (2000), Tectono-sedimentary evolution of active extensional basins, *Basin Res.*, *12*(3-4), 195–218.

Gawthorpe, R. L., A. J. Fraser, and R. E. L. Collier (1994), Sequence stratigraphy in active extensional basins: Implications for the interpretation of ancient basin-fills, *Mar. Pet. Geol.*, *11*(6), 642–658, doi:10.1016/0264-8172(94)90021-3.

Gawthorpe, R. L., C. A. L. Jackson, M. J. Young, I. R. Sharp, A. R. Moustafa, and C. W. Leppard (2003), Normal fault growth, displacement localisation and the evolution of normal fault populations: The Hammam Faraun fault block, Suez rift, Egypt, *J. Struct. Geol.*, *25*(6), 883–895, doi:10.1016/S0191-8141(02)00088-3.

Goldhammer, R. K. (1997), Compaction and decompaction algorithms for sedimentary carbonates, *J. Sediment. Res.*, *67*(1), 26–35.

Gupta, A., and C. H. Scholz (2000), A model of normal fault interaction based on observations and theory, *J. Struct. Geol.*, *22*(7), 865–879, doi:10.1016/S0191-8141(00)00011-0.

Gupta, S., P. A. Cowie, N. H. Dawers, and J. R. A. Underhill (1998), Mechanism to explain rift basin subsidence and stratigraphic patterns through fault array evolution, *Geology*, *26*, 595–598.

Hayward, N. J., and C. J. Ebinger (1996), Variations in the along-axis segmentation of the Afar Rift system, *Tectonics*, *15*(2), 244–257, doi:10.1029/95TC02292.

Hemelsdaël, R., and M. Ford (2014), Relay zone evolution: A history of repeated fault propagation and linkage, central Corinth Rift, Greece, *Basin Res.*, 1–23, doi:10.1111/bre.12101.

Huismans, R. S., and C. Beaumont (2007), Roles of lithospheric strain softening and heterogeneity in determining the geometry of rifts and continental margins, *Geol. Soc. London Spec. Publ.*, *282*(1), 111–138, doi:10.1144/SP282.6.

Jolivet, L., J. M. Daniel, C. Truffert, and B. Goffé (1994), Exhumation of deep crustal metamorphic rocks and crustal extension in arc and back-arc regions, *Lithos*, *33*(1-3), 3–30, doi:10.1016/0024-4937(94)90051-5.

Kornsawan, A., and C. K. Morley (2002), The origin and evolution of complex transfer zones (graben shifts) in conjugate fault systems around the Funan Field, Pattani basin, Gulf of Thailand, *J. Struct. Geol.*, *24*, 435–449.

Le Pourhiet, L., E. Burov, and I. Moretti (2003), Initial crustal thickness geometry controls on the extension in a back arc domain: Case of the Gulf of Corinth, *Tectonics*, *22*(4), 1032, doi:10.1029/2002TC001433.

Leeder, M. R., and G. H. Mack (2009), Basin-fill incision, Rio Grande and Gulf of Corinth Rifts: Convergent response to climatic and tectonic drivers, in *Sedimentary Processes, Environments and Basins*, pp. 9–27, Blackwell, Oxford, U. K.

Leeder, M. R., R. E. L. Collier, L. H. Abdul Aziz, M. Trout, G. Ferentinos, G. Papatheodorou, and E. Lyberis (2002), Tectono-sedimentary processes along an active marine/lacustrine half-graben margin: Alkyonides Gulf, E. Gulf of Corinth, Greece, *Basin Res.*, *14*(1), 25–41, doi:10.1046/j.1365-2117.2002.00164.x.

Leeder, M. R., L. C. McNeill, R. E. L. Collier, C. Portman, P. J. Rowe, J. E. Andrews, and R. L. Gawthorpe (2003), Corinth Rift margin uplift: New evidence from Late Quaternary marine shorelines, *Geophys. Res. Lett.*, *30*(12), 1611, doi:10.1029/2003GL017382.

Leeder, M. R., C. Portman, J. E. Andrews, R. E. L. Collier, E. Finch, R. L. Gawthorpe, L. C. McNeill, M. Perez-Arlucea, and P. Rowe (2005), Normal faulting and crustal deformation, Alkyonides Gulf and Perachora peninsula, eastern Gulf of Corinth Rift, Greece, *J. Geol. Soc. London*, *162*(3), 549–561, doi:10.1144/0016-764904-075.

Leeder, M. R., G. H. Mack, A. T. Brasier, R. R. Parrish, W. C. McIntosh, J. E. Andrews, and C. E. Duermeijer (2008), Late-Pliocene timing of Corinth (Greece) rift-margin fault migration, *Earth Planet. Sci. Lett.*, *274*(1-2), 132–141, doi:10.1016/j.epsl.2008.07.006.

Leeder, M. R., D. F. Mark, R. L. Gawthorpe, H. Kranis, S. Loveless, N. Pedentchouk, E. Skourtsos, J. Turner, J. E. Andrews, and M. Stamatakis (2012), A "Great Deepening": Chronology of rift climax, Corinth Rift, Greece, *Geology*, *40*(11), 999–1002, doi:10.1130/G33360.1.

Lykousis, V., D. Sakellariou, I. Moretti, and H. Kaberi (2007), Late Quaternary basin evolution of the Gulf of Corinth: Sequence stratigraphy, sedimentation, fault–slip and subsidence rates, *Tectonophysics*, *440*(1-4), 29–51, doi:10.1016/j.tecto.2006.11.007.

Manatschal, G., and D. Bernoulli (1999), Architecture and tectonic evolution of nonvolcanic margins: Present-day Galicia and ancient Adria, *Tectonics*, *18*(6), 1099–1119, doi:10.1029/1999TC900041.

Mansfield, C., and J. Cartwright (2001), Fault growth by linkage: Observations and implications from analogue models, *J. Struct. Geol.*, *23*, 745–763.

McKenzie, D. (1972), Active tectonics of the Mediterranean Region, *Geophys. J. Int.*, *30*(2), 109–185, doi:10.1111/j.1365-246X.1972.tb02351.x.

McKenzie, D. (1978), Active tectonics of the Alpine-Himalayan belt: The Aegean Sea and surrounding regions, *Geophys. J. Int.*, *55*(1), 217–254, doi:10.1111/j.1365-246X.1978.tb04759.x.

McNeill, L. C., C. J. Cotterill, T. J. Henstock, J. M. Bull, A. Stefatos, R. E. L. Collier, G. Papatheoderou, G. Ferentinos, and S. E. Hicks (2005), Active faulting within the offshore western Gulf of Corinth, Greece: Implications for models of continental rift deformation, *Geology*, *33*(4), 241–244, doi:10.1130/G21127.1.

McNeill, L., D. Sakellariou, and C. Nixon (2014), Drilling to resolve the evolution of the Corinth Rift, *Eos Trans. AGU*, *95*(20), 170–170, doi:10.1002/2014EO200009.

Mohammed, M., D. Paton, R. E. L. Collier, N. Hodgson, and M. Negonga (2016), Interaciton of crustal heterogeneity and lithospheric processes in determining passive margin architecture on the southern Namibian margin, *Geol. Soc. London Spec. Publ.*, *438*, doi:10.1144/SP438.9.

Moretti, I., V. Lykousis, D. Sakellariou, J. Y. Reynaud, B. Benziane, and A. Prinzhoffer (2004), Sedimentation and subsidence rate in the Gulf of Corinth: What we learn from the Marion Dufresne's long-piston coring, *C. R. Geosci.*, *336*(4-5), 291–299, doi:10.1016/j.crte.2003.11.011.

Morley, C. K. (1999), Patterns of displacement along large normal faults: Implications for basin evolution and fault propagation, based on examples from East Africa, *AAPG Bull.*, *83*, 613–634.

Morley, C. K. (2010), Stress re-orientation along zones of weak fabrics in rifts: An explanation for pure extension in "oblique" rift segments? *Earth Planet. Sci. Lett.*, *297*(3-4), 667–673, doi:10.1016/j.epsl.2010.07.022.

Morley, C. K., P. Vanhauwaert, and M. De Batist (2000), Evidence for high frequency cyclic fault activity from high resolution seismic reflection survey, Rukwa Rift,Tanzania, *J. Geol. Soc. London.*, *157*, 983–984.

Nelson, R. A., T. L. Patton, and C. K. Morley (1992), Rift-segment interaction and its relation to hydrocarbon exploration in continental rift systems, *AAPG Bull.*, *76*, 1153–1169.

Nixon, C. W., D. J. Sanderson, and J. M. Bull (2011), Deformation within a strike-slip fault network at Westward Ho!, Devon U.K.: Domino vs conjugate faulting, *J. Struct. Geol.*, *33*(5), 833–843, doi:10.1016/j.jsg.2011.03.009.

Nixon, C. W., J. M. Bull, and D. J. Sanderson (2014), Localized vs distributed deformation associated with the linkage history of an active normal fault, Whakatane Graben, New Zealand, *J. Struct. Geol.*, *69*, 266–280, doi:10.1016/j.jsg.2014.06.005.

Ori, G. G. (1989), Geologic history of the extensional basin of the Gulf of Corinth (?Miocene-Pleistocene), Greece, *Geology*, *17*(10), 918–921, doi:10.1130/0091-7613(1989)017<0918:GHOTEB>2.3.CO;2.

Paton, D. A. (2006), Influence of crustal heterogeneity on normal fault dimensions and evolution: Southern South Africa extensional system, *J. Struct. Geol.*, *28*(5), 868–886.

Paton, D. A., D. I. M. Macdonald, and J. R. Underhill (2006), Applicability of thin or thick skinned structural models in a region of multiple inversion episodes; southern South Africa, *J. Struct. Geol.*, *28*(11), 1933–1947, doi:10.1016/j.jsg.2006.07.002.

Patton, T. L., A. R. Moustafa, R. A. Nelson, and S. A. Abdine (1994), Tectonic evolution and structural setting of the Suez Rift: Chapter 1: Part I. Type basin: Gulf of Suez, Interior rift basins, *Am. Assoc. Petrol. Geol. Mem.*, 59, 9–55.

Peacock, D. C. P., and D. J. Sanderson (1991), Displacements, segment linkage and relay ramps in normal fault zones, *J. Struct. Geol.*, *13*(6), 721–733, doi:10.1016/0191-8141(91)90033-F.

Perissoratis, C., D. J. W. Piper, and V. Lykousis (2000), Alternating marine and lacustrine sedimentation during late Quaternary in the Gulf of Corinth rift basin, central Greece, *Mar. Geol.*, *167*, 391–411.

Ranero, C. R., and M. Pérez-Gussinyé (2010), Sequential faulting explains the asymmetry and extension discrepancy of conjugate margins, *Nature*, *468*(7321), 294–9, doi:10.1038/nature09520.

Roberts, G. P., S. L. Houghton, C. Underwood, I. Papanikolaou, P. A. Cowie, P. van Calsteren, T. Wigley, F. J. Cooper, and J. M. McArthur (2009), Localization of Quaternary slip rates in an active rift in 10 5 years: An example from central Greece constrained by 234 U-230 Th coral dates from uplifted paleoshorelines, *J. Geophys. Res.*, *114*, B10406, doi:10.1029/2008JB005818.

Roberts, S., and J. Jackson (1991), Active normal faulting in central Greece: An overview, *Geol. Soc. London Spec. Publ.*, *56*(1), 125–142, doi:10.1144/GSL.SP.1991.056.01.09.

Rohais, S., R. Eschard, M. Ford, F. Guillocheau, and I. Moretti (2007), Stratigraphic architecture of the Plio-Pleistocene infill of the Corinth Rift: Implications for its structural evolution, *Tectonophysics*, *440*(1-4), 5–28, doi:10.1016/j.tecto.2006.11.006.

Rosendahl, B. R. (1987), Architecture of continental rifts with special reference to East Africa, *Annu. Rev. Earth Planet. Sci.*, *1987*, 445–503.

Sachpazi, M., C. Clément, M. Laigle, A. Hirn, and N. Roussos (2003), Rift structure, evolution, and earthquakes in the Gulf of Corinth, from reflection seismic images, *Earth Planet. Sci. Lett.*, *216*(3), 243–257, doi:10.1016/S0012-821X(03)00503-X.

Sakellariou, D., V. Lykousis, S. Alexandri, H. Kaberi, G. Rousakis, P. Nomikou, P. Georgiou, and D. Ballas (2007), Faulting, seismic-stratigraphic architecture and Late Quaternary evolution of the Gulf of Alkyonides Basin-East Gulf of Corinth, Central Greece, *Basin Res.*, *19*(2), 273–295, doi:10.1111/j.1365-2117.2007.00322.x.

Schlische, R. W. (1993), Anatomy and evolution of the Triassic-Jurassic Continental Rift System, eastern North America, *Tectonics*, *12*(4), 1026–1042, doi:10.1029/93TC01062.

Schlische, R. W., and M. O. Withjack (2009), Origin of fault domains and fault-domain boundaries (transfer zones and accommodation zones) in extensional provinces: Result of random nucleation and self-organized fault growth, *J. Struct. Geol.*, *31*(9), 910–925, doi:10.1016/j.jsg.2008.09.005.

Skourlis, K., and T. Doutsos (2003), The Pindos fold-and-thrust belt (Greece): Inversion kinematics of a passive continental margin, *Int. J. Earth Sci.*, *92*(6), 891–903, doi:10.1007/s00531-003-0365-4.

Skourtsos, E., and H. Kranis (2009), Structure and evolution of the western Corinth Rift, through new field data from the Northern Peloponnesus, *Geol. Soc. London Spec. Publ.*, *321*(1), 119–138, doi:10.1144/SP321.6.

Soliva, R., and R. A. Schultz (2008), Distributed and localized faulting in extensional settings: Insight from the North Ethiopian Rift–Afar transition area, *Tectonics*, *27*, TC2003, doi:10.1029/2007TC002148.

Stefatos, A., G. Papatheodorou, G. Ferentinos, M. Leeder, and R. Collier (2002), Seismic reflection imaging of active offshore faults in the Gulf of Corinth: Their seismotectonic significance, *Basin Res.*, *14*(4), 487–502, doi:10.1046/j.1365-2117.2002.00176.x.

Taylor, B., J. R. Weiss, A. M. Goodliffe, M. Sachpazi, M. Laigle, and A. Hirn (2011), The structures, stratigraphy and evolution of the Gulf of Corinth Rift, Greece, *Geophys. J. Int.*, *185*(3), 1189–1219, doi:10.1111/j.1365-246X.2011.05014.x.

Taylor, S. K., J. M. Bull, G. Lamarche, and P. M. Barnes (2004), Normal fault growth and linkage in the Whakatane Graben, New Zealand, during the last 1.3 Myr, *J. Geophys. Res.*, *109*, B02408, doi:10.1029/2003JB002412.

Tiberi, C., et al. (2000), Crustal and upper mantle structure beneath the Corinth Rift (Greece) from a teleseismic tomography study, *J. Geophys. Res.*, *105*(B12), 28,159–28,171, doi:10.1029/2000JB900216.

Walsh, J. J., et al. (2001), Geometric controls on the evolution of normal fault systems, *Geol. Soc. London Spec. Publ.*, *186*(1), 157–170, doi:10.1144/GSL.SP.2001.186.01.10.

Walsh, J. J., A. Nicol, and C. Childs (2002), An alternative model for the growth of faults, *J. Struct. Geol.*, *24*, 1669–1675.

Walsh, J. J., W. R. Bailey, C. Childs, A. Nicol, and C. G. Bonson (2003a), Formation of segmented normal faults: A 3-D perspective, *J. Struct. Geol.*, *25*(8), 1251–1262, doi:10.1016/S0191-8141(02)00161-X.

Walsh, J. J., C. Childs, J. Imber, T. Manzocchi, J. Watterson, and P. A. R. Nell (2003b), Strain localisation and population changes during fault system growth within the Inner Moray Firth, Northern North Sea, *J. Struct. Geol.*, *25*(2), 307–315, doi:10.1016/S0191-8141(02)00028-7.

Wilson, P., D. Hodgetts, F. Rarity, R. L. Gawthorpe, and I. R. Sharp (2009), Structural geology and 4D evolution of a half-graben: New digital outcrop modelling techniques applied to the Nukhul half-graben, Suez rift, Egypt, *J. Struct. Geol.*, *31*(3), 328–345, doi:10.1016/j.jsg.2008.11.013.

Wilson, R. C. L., G. Manatschal, and S. Wise (2001), Rifting along non-volcanic passive margins: Stratigraphic and seismic evidence from the Mesozoic successions of the Alps and western Iberia, *Geol. Soc. London Spec. Publ.*, *187*(1), 429–452, doi:10.1144/GSL.SP.2001.187.01.21.

Wood, A. M., D. A. Paton, and R. E. L. Collier (2015), Understanding regional scale structural uncertainty: The onshore Gulf of Corinth Rift as a hydrocarbon exploration analogue, *Interpretation*, *3*(4), SAC35–SAC53.

Zelt, B. C., B. Taylor, J. R. Weiss, A. M. Goodliffe, M. Sachpazi, and A. Hirn (2004), Streamer topography velocity models for the Gulf of Corinth and Gulf of Itea, Greece, *Geophys. J. Int.*, *159*, 333–346.